ISSN-1996-918X

Pak. J. Anal. Environ. Chem. Vol. 25, No. 2 (2024) 150 – 182

http://doi.org/10.21743/pjaec/2024.12.01

Review

Synthesis, Properties and Applications of Lead Halide Perovskite Nanocrystals

Aisha Shamim[1], Hasan Abdulnaser Charam[2], Gul E Nayyab[3] and Monis Bin Abid[2]*

[1]*Department of Chemistry, University of Wah, Wah Cantt, Pakistan.*

[2]*Department of General Studies, University of Prince Mugrin, Madinah Al Munawara, Saudi Arabia.*

[3]*Department of Technology & Natural Resources, Faculty of Applied Science and Technology, Universiti Tun Hussein Onn Malaysia, Pagoh Education Hub, 84600 Muar, Johor, Malaysia.*

*Corresponding author Email: m.abid@upm.edu.sa

Received 07 November 2023, Revised 06 August 2024, Accepted 03 September 2024

Abstract

Owing to superb optical versatility, soaring photoluminescence quantum yields, and simple fabrication, perovskite nanocrystals have captivated the interest of researchers across the globe. They are one of the most promising materials of the 20th century due to their extensive applications in optoelectronic devices, such as solar cells, flat panel displays, solid-state lighting, detectors, photovoltaics, and sensor fields. The critical attribute of lead halide perovskite nanocrystals (LHPNCs) is the innocuous nature of their structural defects, although highly abundant in these compounds relative to their optical and electronic properties. The structure of halide perovskite is responsible for its excellent optoelectronic properties, including a high absorption coefficient, huge photoluminescence quantum yield (PLQY), pure color emission, and tunable band gap. The emergence of novel colloidal synthetic strategies for the fabrication of halide perovskite NCs and the exciting properties of this new type of material have attracted the focus of many researchers. This paper provides a comprehensive overview of perovskite nanocrystals (PNCs), covering synthesis methods, properties, stability challenges, and potential applications. It examines several methodologies, such as hot injection, ligand-assisted reprecipitation (LARP), and ion exchange techniques, along with exploring PNCs characteristics such as crystal structure and defect tolerance. Strategies for enhancing stability and utilizing LHPNCs in optoelectronics and photovoltaics are also discussed.

Keywords*:* Perovskite nanocrystals, Hot Injection, Crystal size, PLQY, Solar cells

Introduction

LHPNCs are ancient substances that were first synthesized in 1893, and their structure was described entirely in the late 1950s. Traditionally, the isostructural oxide ABO_3 compounds such as $CaTiO_3$ have been referred to as perovskites. Their general formula is ABX_3, where A is methylammonium (MA), formamidinium (FA), or cesium (Cs): B symbolizes lead (Pb) or tin (Sn), and X is any of the halide ions (chloride (Cl^-), bromide (Br-), or iodide (I^-). (Pb) is surrounded by six halide anions (Cl^-, Br^-, or I^-) located at the vertices, creating octahedrons coordinated in a six-fold manner that expand into a three-dimensional framework through vertex connections. The Perovskite configuration relies on electrostatic interactions to stabilize the overall charge, thereby generating anionic corner-linked inorganic octahedra through covalent bonding alongside organic cations

positioned within the cuboctahedral void [1]. Gustav Rose and Lev Perovski discovered the naturally occurring mineral $CaTiO_3$ in 1938 in the Ural Mountains [2]. In 1970, Weber [3] completed the synthesis of the $MAPbX_3$ and determined their crystal structure . Since then, all $APbX_3$ family members have been obtained as solution-grown single crystals, and their whole structure has been described. In 1958, Moller discovered the first perovskite structure in $CsPbX_3$ [4]. In 1990, Mitzi et al. concentrated on layered organic-inorganic perovskites, which were used in thin-film transistors and light-emitting diodes (LEDs) because of their potent excitonic characteristics [5]. Pioneering work on halide perovskite photovoltaic was done by Miyasaka et al. [6] As early as 2005, this group began developing perovskite solar cells [6, 7]. Then, in 2006, hybrid perovskite made its photovoltaic debut. Altering Br^- with I^-, a peak power conversion efficiencies (PCEs) of 3.8% was procured in 2009 [8]. Lee et al. [9] showed that using solid electrolytes as a hole transport layer (HTL) resulted in an efficiency of 10.9%.

Although Perovskites are old materials, they spurred the interest of the optoelectronic community in recent years [10]. Kojima et al. [11] were pioneers who originally developed $CH_3NH_3PbI_3$ as a sensitizer in 2009. A band gap (1.55eV) is an adequate light absorber across the visible spectrum. Because of their lucrative synthesis, solution manufacturing, and exceptional optoelectronic characteristics, LHPNCs have become auspicious semiconductors. These materials have rendered applications in optical and electronic devices like LEDs, lasers, photodetectors, and solar cells [12]. Early research utilized LHPNCs as the primary active layers, and the solar cells' PCEs quickly increased from (3.8- 25.5%) [13,14]. Quantum efficiencies of LEDs were increased from < 1% to over 20% [15]. When the size is reduced to nanometer and non-radiative channels are suppressed to perfection, then an outstanding direct-band gap semiconductor material typically exhibits unusual photophysical properties, according to research on typical colloidal semiconductor nanocrystals like CdSe and InP [14]. In 2011 Park and coworkers [15] attained 6.5% PCE using Perovskite quantum dots (QDs) as sensitizers. Following the advancements in incredibly competent Perovskite solar cells, materials scientists, chemists, and physicists concentrated their efforts on synthesizing, characterization, and applications of LHPNCs with the objectives of increasing their PLQs as well as getting an understanding of their remarkable optical characteristics in the quantum-confinement system [1, 15]. PNCs are prone to degradation, and their inherent instability comes from low formation energy and sensitivity to moisture, light, and oxygen. The instability of Perovskite nanomaterial is a substantial hurdle in the practical applications of Perovskite LEDs despite their recent rapid progress. So far, convincing development has been made in improving the stability of lead halide PNCs, including compact barrier matrix encapsulation, polymeric matrices, and surface engineering strategies [16].

However, lead halide perovskites (LHPs) are highly defect-tolerant materials, unlike classical semiconductors, such as Si, GaAs, CdTe, CdSe, and InP, where usually lesser defects lead to highly detrimental results for PLQY and charge carrier mobility. Thus, the optical and optoelectronic properties of LHPs are not affected. The defect tolerance of LHPs leads to the amalgamation of Perovskite solar cells having high efficiency with polycrystalline films; their crystallization occurs at relatively low

temperatures and ambient conditions and possesses a high density of defects [17].

In recent years, substantial endeavors have been employed to develop straightforward and consistent fabrication strategies for metal halide Perovskites. Among all fabrication procedures, halide ion (HI) and LARP have been the most exploited methods for fabricating metal halide perovskite nanocrystals (MHPNCs). The HI method generally produces high-quality monodisperse $CsPbX_3$ NCs with high PLQY. Over the years, the HI approach of metal halide PNCs has developed, and it is being used with various precursors and ligands, leading to better stability and shape control. However, this strategy needs high temperatures and inert atmospheres, which is not cost-effective. The reprecipitation approach has been exploited to synthesize organic nanoparticles and has been known for centuries. The basic principle involves the spontaneous crystallization of materials in the supersaturated state, which can be achieved by reduction, evaporation, and addition of temperature, solvent, or a poor solvent in which the solubility of the substance is low, respectively. If this occurs when ligands are present, nucleation and growth of the residue can be regulated, and this is called the LARP approach [18].

This review paper aims to offer a comprehensive and systematic analysis of PNCs, focusing on their synthesis techniques, stability challenges, and possible uses. Through an examination of various synthesis methods such as hot injection, LARP approach, halide ion exchange, cation exchange, solid-state, and gas-state synthesis techniques, the aim of this paper is to clarify the processes and conditions that impact the quality and attributes of PNCs. Furthermore, it investigates the fundamental characteristics of PNCs, such as crystal structure, optical and electronic properties, and defect tolerance, which are essential for their effectiveness in diverse applications. It also discusses the structural vulnerabilities and stability concerns inherent in PNCs, proposing approaches to improve their stability and efficiency.

Synthesis of Perovskite Nanocrystals

A substantial effort was put into establishing dependable and simple synthetic methods to manufacture high-quality LHPNCs that have control over size morphology and optical traits. These methods can be divided into "top-down" and "bottom-up" categories. In top-down methods, fragmentation, assembling [19], or chemical exfoliation [20] is performed, whereas in bottom-up techniques, molecules and ions undergo chemical processes in the liquid or gas phase. It has been established that the liquid-phase technique is the most effective bottom-up strategy for producing well-defined colloidal PNCs [21]. In 2014, the first colloidal synthesis of LHPNCs, was studied in which Methylammonium lead tribromide ($MAPbBr_3$) NCs were made stable by a long or moderate chain alkyl ammonium bromide [22]. These NPs were created by reacting MABr and $PbBr_2$ in the presence of 1-octadecene and oleic acid [20]. This groundbreaking statement made it feasible to spin coat these nanoparticle solutions to create homogeneous LHPNCs thin films. To create $MAPbX_3$ PNCs at room temperature, Zhang et al. [23] first showed a LARP technique a year later , which involves the addition of the mixture of MAX, PbX_2, olylamine, and oleic acid in a polar solvent like DMF, the nucleation and development steps came about in toluene (a less polar solvent). The difference between these precursors' solubilities before and after solvent mixing caused them to change into crystalline colloidal nanoparticles. LARP was widely used to create several different colloidal perovskite nanocrystals [22]. However, the hot-injection technique, which Protesescu et

al. disclosed in 2015, was what truly spurred research on LHPQDs, specifically all-inorganic ($CsPbX_3$) NCs. On the other hand, the HI approach necessitates extreme temperature and inert conditions, resulting in cost hikes and yield reduction [24]. The LARP approach, which produces superior PNCs at room temperature, can be used as a more economical substitute to overcome these potential drawbacks [25].

Hot Injection Method

The first Hot Injection Method (HIM) was developed over 25 years ago to synthesize the first cadmium chalcogenide nanocrystals [26]. This method relies on quickly injecting a precursor into a heated mixture of the precursors with ligands and a solvent having a sharp boiling point [27]. By separating the nucleation and development processes, the HIM is often employed to fabricate minute nanocrystals with a narrow size distribution [28]. A quick nucleation burst and the simultaneous production of tiny nuclei happen immediately after the injection. Nucleation is abruptly ended by fast monomer attenuation, after which the nuclei expand. This causes the population of NCs to evolve and become identifiable [29]. To supervise the size and shape of colloidal PNCs, the ratio of surfactants to precursors, the temperature of injecting precursors, the reaction time, and the amount of precursors are crucial. The hot injection strategy for the fabrication of NPs was expanded in 2015 to enable the colloidal production of cesium LHP ($CsPbX_3$) [29]. These NCs were fabricated by injection of cesium-oleate into a heated PbX_2 salt solution solubilized in ODE, carboxylic acids, and amines (Fig. 1). It was reported that equal ratios of primary amines and carboxylic acids led to the amalgamation of monodisperse PNCs. Mixed-halide perovskites could also be favorably fabricated by fixing the ratios of $PbCl_2$ and $PbBr_2$ or $PbBr_2$ and PbI_2 salts. The photoluminescence emission of the thus formed nanocrystals could be calibrated beyond all visible spectrums by fluctuating the composition of halides or by varying the size of nanocrystals. The hot injection method was then applied to synthesize $MAPbX_3$ NCs by interchanging Cs-oleate with a methylamine solution [30]. By balancing the ratio of the OLA and OA, $MAPbBr_3$ and $MAPbI_3$ PNCs were successfully fabricated.

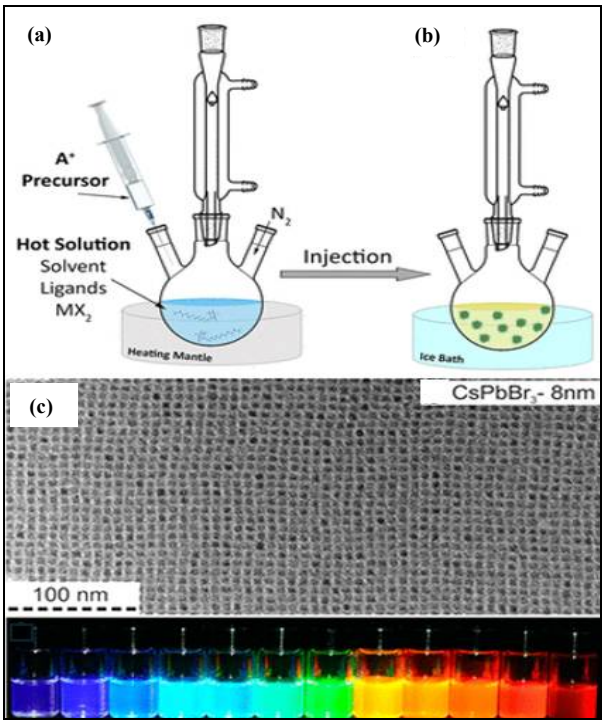

Figure 1. **(a) Graphical representation of colloidal HI strategy applied to synthesize MHPNCs. (b) TEM image of $CsPbBr_3$ NCs fabricated by HI. (c) $CsPbX_3$ (X = Cl, Br, I) PNC dispersions in vials with different halide compositions in solvent toluene under UV. It is reproduced from ref [32] Copyright 2019 American Chemical Society**

The HIM was further refined to produce materials based on lead halide linked to perovskites. When manipulating cesium ions or working under conditions enriched with olylamine, Cs_4PbX_6 nanocrystals were adequately synthesized. The produced nanocrystals were quite monodispersed, with the size tuned from 9 nm to 37 nm [31]. By using microfluidic technology, Lignos et al. [32] gained insight into the growth dynamics

of $CsPbX_3$ nanocrystals created using the HI method. The $CsPbX_3$ NCs' in situ absorption and photoluminescence demonstrated that the nucleation and growth occurred in the first 1–5 seconds of the chemical reaction, demonstrating the high response rate of these NCs. Koolyk et al. [31], who examined the rate of growth of $CsPbBr_3$ and $CsPbI_3$ PNCs by obtaining fractions at various phases of the process and studying them TEM, reported slightly different findings. In $CsPbI_3$ NCs, they saw that the size-focusing mechanism only persisted for the first 20 seconds before giving way to a size-defocusing mechanism. However, they discovered that the thickness of $CsPbBr_3$ PNCs was not defined by any size focusing mechanism; instead, it was characterized from the start by extension of the percentage of the size of particles, and this continued during the entire reaction period of 40s [33]. Udayabhaskararao et al. [34] subsequently presented a two-step growth mechanism after utilizing electron microscopy to track the development of $CsPbX_3$ NCs at various stages. PbO NCs are created in the initial step and serve as the grains on which $CsPbX_3$ NCs nucleate. Self-assembly and directed attachment are the second steps in developing PNCs. Nevertheless, none of these researchers have proven the early genesis of PbO NCs. Furthermore, it is now widely known that when NCs are viewed under an electron microscope, PbO clusters are created by irradiating their periphery with the electron beam [35]. As a result, this mechanism can be disregarded. In general, there is a large diversity in the quality of the perovskite nanocrystals, which shows that unlike traditional hot-injection procedures employed to yield II−VI, IV−VI, III−V, and I−III−VI quantum dots, the nucleation and development stages of perovskite NCs are rapid and practically distinguishable in time. The main challenge that hinders the investigation and application of the attributes of $CsPbX_3$ NCs is the difficulty in manipulating the nucleation and the development with a high homogeneity [36]. Nevertheless, a new study has shown that this problem can be addressed by working under a thermodynamically controlled atmosphere [37]. The highly soluble nature of colloidal lead halide PNCs in polar liquids is a significant drawback for halide perovskites. This indicates that they are unstable in ambient air conditions, such as those with fluctuating humidity, heat, or light, which decreases their PLQY [24].

Yuan et al. [36] demonstrated that the high solubility of colloidal lead halide PNCs in polar liquids poses a significant drawback for their stability. Woo et al. [37] discovered that working in halide-rich circumstances can significantly increase the stability of $CsPbX_3$ NCs without a noticeable lowering in the PLQY, which is necessary to offset the stripping of halide ions that comes along with the usage of polar antisolvents [38]. Besides the $PbBr_2$ precursor, $ZnBr_2$ was used in that study as an additional reservoir of bromide, an ion. In comparison to NCs created without the use of metal bromide, the final products had compositions that were more halide-rich. According to the authors, this method represents the first successful attempt at in situ inorganic passivation stabilizing $CsPbX_3$ NCs [39]. Using metal halide salts as precursors is a significant shortcoming of the HIM, as discussed, and this restricts the possible ways to work with the appropriate ion stoichiometry [40]. To eliminate these limitations, Liu et al. [39] introduced the “three-precursor" HIM for amalgamating $CsPbX_3$ NCs. Instead of employing the more traditional PbX_2 salts, they used NH_4X and PbO as reservoirs of X^- and Pb^{+2} ions, as previously reported [37]. Compared to normal NCs, the $CsPbBr_3$ NCs produced using an excess of NH_4Br under Br-rich conditions had better optical characteristics and a remarkable improvement in stability as they successfully

passed through the purification step. By removing alkylamines from the synthesis, Yassitepe et al. [40] improved the three-precursor hot injection method and manufactured oleic acid (OA) capped $CsPbX_3$ NCs. In their method, quaternary alkylammonium halides, including tetraoctyl-ammonium halides that cannot generate ammonium species having protons, reacted with Cs-acetate and Pb-acetate. It was shown that the growth kinetics were significantly sped up in the absence of olylamine, allowing the fabrication of $CsPbX_3$ PNCs to occur at a lower temp (75 °C). The $CsPbBr_3$ NCs produced using this method had PLQYs of up to 70% and improved colloidal stability. However, this approach could not create $CsPbI_3$ NCs with the same quality and stability [20]. Later, Protesescu et al. [41] used and modified the HI three-precursor method for the colloidal fabrication of $FAPbX_3$ PNCs. In essence, formamidinium (FA) and Pb acetates were combined with oleic acid in1-octadecene (ODE) to create $FAPbBr_3$ NCs, which were then injected with oleylammonium bromide. The end product also included a 5–10% byproduct of $NH_4Pb_2Br_5$, which may have been created during the synthesis when FA^+ was thermally converted to NH_4^+. By reaction between FA-oleate and PbI_2 complex with oleic acid and olylamine in ODE and an excess amount of FA, highly pure $FAPbI_3$ PNCs with advanced optical quality were auspiciously fabricated in 2017. Since the sources of the metal ions and halides are not connected, the three-precursor HI technique enables the chosen stoichiometry of ions. Still, it makes this technique less versatile as it has several drawbacks. It has been understood that this method is not suitable for fabricating $CsPbI_3$, $CsPbCl_3$, and $MAPbX_3$, where x stands for Br and I PNCs, which shows that the precursors (halides) do not react appropriately in the reaction circumstances of this method [42].

In addition, many undesirable secondary steps linked to the breakdown of the alkyl ammonium halide were discovered during the production of $FAPbX_3$ nanocrystals [43]. Imran et al. [44]ecently disclosed novel techniques to address the drawbacks of the three precursors of HIM strategies, and Creutz et al. [43] used almost the same approach. These methods rely on the employment of quickly injected extremely reactive halides, such as in a solution of metal carboxylates. The PNCs instantly start to develop and nucleate after injection. With high dominance over the size and purity of phase. Imran et al. [44] and Tong et al. [45] exploited benzoyl halides as a reservoir of X^- ions and manipulated to construct a full pedigree of all-inorganic and hybrid lead halide PNCs [46]. Like this, Creutz et al. [43] created Cs_2AgBiX_6 nanocrystals using trimethylsilyl halides. The ability to use appropriate ratios of cations and anions, especially in an environment enriched with halide ions, is of particular value. For example, $CsPbCl_3$ PNCs were fabricated using LARP or the two-precursor HI methods and were analyzed by considerable nonradiative recombination. It was reported to efficiently boost the PLQY of the resultant PNCs in various situations [47]. While using too much benzoyl chloride increased their PLQY to a record high of 65% [48]. The difficulty of the purification procedures required to remove 1-octadecene and non-reacting materials is a significant defect in the HI approach. Also, perovskite NCs show sensitivity to the antisolvents used in the cleaning procedure. Various anti-solvents, such as isopropanol, butanol, and acetone, can draw halide ions into solution during the process of purifying PNCs, as demonstrated in Yuan et al. 's work [36], which considerably changes the optical characteristics of $CsPbX_3$ NCs (X is I or Br or their mixture) [49].

LARP Approach

Since salt recrystallization first took place in clay pots in South Poland about 3500 BC, the technique of supersaturated recrystallization has been around for more than 5000 years [29]. In this process, the required ions are dissolved in a solvent. After attaining equilibrium concentration, the solution is transferred into a supersaturation condition. One can change the temperature (chilling), evaporate the solvent, or add a miscible co-solvent with low ion solubility to achieve a supersaturated state. When this happens, the system experiences involuntary precipitation and crystallization reactions until it returns to equilibrium. In the 1990s, this method was expanded to create polymer dots and organic nanoparticles [50]. The production of crystals and their growth can be supervised to the nano range when this process occurs in the presence of ligands. The LARP method, when used for the amalgamation of nanocrystals, merely entails mixing the required precursor in the proximity of ligands in a poor solvent like toluene or hexane after dissolving them in a suitable polar solvent, such as DMF or DMSO. The salts MX_2, CsX, MAX, and FAX are frequently utilized in the LARP technique. When the two solvents are combined, an abrupt supersaturation results, causing perovskite NCs to form and increase. Being that the LARP method is performed in air using a relatively primary chemical material as opposed to the hot injection approaches, it is evident that it can be scaled up quickly, enabling the fabrication of metal halide PNCs on a commercial scale [22]. Nucleation and growth in LARP cannot be distinguished, just as they cannot be in the hot injection procedures [51].

In 2012, Nikaki et al. [52] dissolved $MAPbX_3$, (MA) $(CH_3C_6H_4CH_2NH_3)_2$ Pb_2X_7, or (MA) $(C_4H_9NH_3)_2$ Pb_2X_7 salts in DMF, which is an aprotic solvent [53] , then drizzled the corresponding solutions in toluene or a mixture of toluene and poly(- methyl methacrylate) (PMMA) and this was the first statement on LARP based fabrication of (HOP) [52]. They saw the emergence of luminous NCs between 30 and 160 nm in size and had PL intensities significantly greater than those predicted for their bulk equivalents. Then, more time was taken by the LARP method to establish the fabrication of (OI) $MAPbX_3$ NCs. Zhang et al. [23] introduced the first LARP method to create (OI) $MAPbBr_3$ NCs in 2015. They dissolved $PbBr_2$ and MABr salts in alkyl amines, carboxylic acids, and DMF and developed a precursor solution. Then, to create colloidal NCs, a predetermined quantity of this solution was drizzled in toluene while vigorously stirred. Different amines and acids were investigated to comprehend their precise function. Interestingly, the production of $MAPbBr_3$ NCs was still possible without using amines, but having control over the crystal size was challenging. Also, the aggregated NCs were the outcome of eliminating carboxylic acids from the synthesis. These controlled trials led the authors to conclude that amines regulated the speed of crystallization and, so, the size of the nanocrystals. In contrast, carboxylic acids were believed to prevent aggregation of nanocrystals. In the coming years, several groups exploited and improved this basic strategy [54].

Arunkumar et al. [49] reported that $MAPbX_3$ NCs can be doped with Mn^{2+} by merely incorporating $MnCl_2$ into the precursor solution. Later, it was established that other ligands functioned effectively during the fabrication of $MAPbBr_3$ nanocrystals in the LARP technique [55], demonstrated that 2-adamantylammonium bromide might substitute OLA and OA as the only capping ligand to enhance the optical characteristics of the NCs by using (APTES) and (NH_2-POSS)

[56]. It was claimed that there is more control over the size distribution of the NCs because APTES and NH_2-POSS may prevent the generated NCs from being broken down by DMF. Thus, they offer more stability and uniformity than straight-chain ligands like OA or OABr [57]. In addition to octylamine and OA, benzoyl alcohol was first used by as an auxiliary ligand, and it hastened the rate of reaction and enhanced the optical characteristics of the resultant NCs [58]. In manufacturing $MAPbBr_3$ NCs, Luo et al. [58] used peptides, specifically 12-aminododecanoic acid, as the sole ligand. The size of the generated NCs might be effectively controlled by using peptides that include both NH_2 and COOH groups [59]. Minor modifications were also suggested to enhance the efficiency of the LARP procedure further. For instance, Shamsi et al. [21] developed a different LARP strategy in which they dissolved PbX_2 salts in NMP rather than the usual DMF in the presence of OLA and OA. After 10 minutes of heating to 100 °C, the solution was added dropwise at room temperature to a subpar solvent (dichlorobenzene or chloroform) [60]. The benefit of this method is that MA^+ ions are produced in situ by the transamidation process, eliminating the requirement for earlier MAX salt synthesis (Fig. 2). It is to be noted that the same strategy might produce bulk crystals at RT without the requirement of an antisolvent [60]. Using a spray to combine excellent and poor solvents, Dai et al. [55] created $MAPbBr_3$ NCs with a favorable size distribution [61]. The precursor and subpar solvents were mixed in this method. The spray solution's micrometer-sized droplets offer substantial contact between the two solutions, facilitating a more uniform mixing. Levchuk et al. [19] presented the first LARP method for fabricating $FAPbX_3$ PNCs. They employed a similar synthesis method to create $MAPbX_3$ PNCs, which they had used earlier [62] but made a few minor adjustments [63].

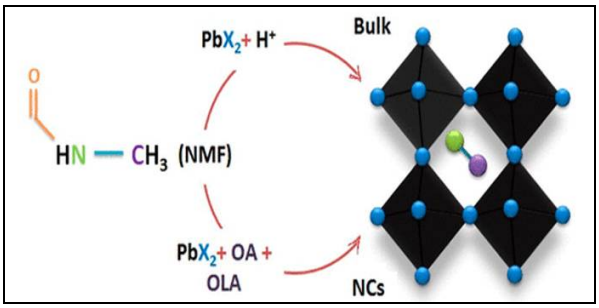

Figure 2. **Exploiting NMF As An MA^+ Source For Fabricating Both PNCs And Bulk Crystals Using Two Synthesis Approaches. Reproduced from ref [32] copyright 2019 American Chemical Society**

The synthesis requires the quick injection precursor solution formed from dissolving PbX_2 and FAX salts in DMF and dissolving OA and OLA into chloroform at RT (Fig. 3 panels a and b). The authors could produce either thickness control nanocubes or NPLs in the 2 to 4 monolayer range by employing OLA and OA ratio as a controlling factor (Fig. 3 panels c and d). An interesting phenomenon was the discovery that toluene caused hindrance to the formation of $FAPbI_3$ NCs, which resulted in the instant agglomeration of $FAPbBr_3$ or $FAPbCl_3$ PNCs.

Minh et al. [57] reported that the production of $FAPbX_3$ nanocubes used new precursors like PbX_2 and DMSO complexes simultaneously. In their method, the PbX_2-DMSO complex, FAX, and OLA were used, and all these materials were solubilized in DMF with the addition of OLA, and the resulting solution was then mixed with a mixture of toluene and OA. It is thought that the creation of $FAPbX_3$ NCs happens due to an exchange reaction in which alkyl ammonium halides can replace the DMSO molecules in the initial PbX_2-DMSO complex. By altering the amount of OLA, the distribution of the size of nanocrystals was better controlled [64]. It presented a significantly changed LARP process to produce $FAPbBr_3$ NPLs with an excellent PLQY that might be employed in LEDs. This experiment created two separate polar

solutions by dissolving salts (FABr, $PbBr_2$) in C_2H_5OH and DMF. These solutions were then introduced concurrently to a combination of toluene, OA, and octylamine [65]. Until 2015, only the hot-injection method could be used to create all-inorganic $CsPbX_3$ PNCs [23]. Liu et al. [39] reported in 2016 that the LARP method could also be performed at RT to create all-inorganic PNCs in colloidal form. The only difference in their synthesis from that of the organic-inorganic $MAPbX_3$ NC complexes is the substitution of CsX for MAX in the precursor solution [66]. Additionally, during this process, OLA and OA were dissolved in DMF together with the inorganic salts and then mixed with toluene, which caused NCs to develop right away. It was improved this strategy by further engineering for controlling the shape of $CsPbX_3$ PNCs. They discovered that changing the poor solvent (toluene) with ethyl acetate, the percentage of ligands, and the reaction time could change the shape of the NCs. When ethyl acetate is used as a solvent, it encourages the synthesis of quasi-cubic QDs, NPLs, and nanobars. In contrast, when toluene is used, it forms nanocubes nanorods (NRs), or nanowires (NWs) [67]. The authors anticipated that the various ligand/nonpolar solvent interactions were responsible for these multiple morphologies. Since ethyl acetate has a high polarity, it functions as a solvent and a nucleophile, leading some OLA molecules to separate from the periphery of the developing nuclei. Thus, the nuclei undergo an oriented attachment. The surfaces of nanocrystals in toluene become more shielded in all orientations if the OLA concentration is high enough, which subsequently causes limitations in their attachment and growth.

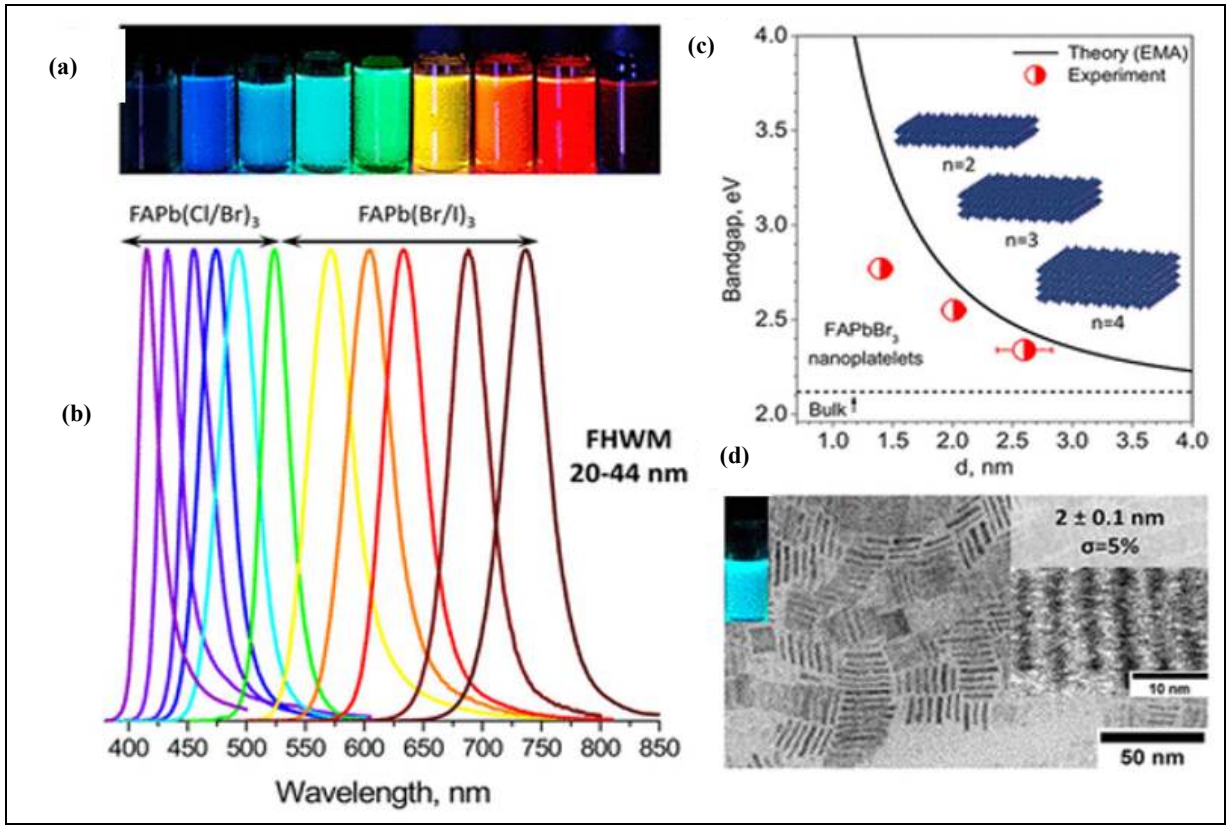

***Figure 3*. (a) Dispersions of $FAPbX_3$ PN under UV light and (b) the emission curves for PL. (c) band gaps of $FAPbBr_3$ NPLs and their effective mass approximation versus thickness. (d) TEM photograph for $FAPbBr_3$ NPLs. Reproduced with permission from ref [32]. Copyright 2019 American Chemical Society**

There is a phenomenon of anisotropy involved in the growth of PNCs, which, when grown in the form of NRs and NWs, take longer reaction times if only a tiny quantity of OLA is added to the toluene. This is most likely due to the facets' surfaces not being completely passivated. Kostopoulou et al. [60] used LARP to synthesize micron-sized $CsPbBr_3$ NWs 2017. Anhydrous solvents were used in this method, which are crucial components besides low temperature. This method involves dropping the precursor solution with CsBr, $PbBr_2$, DMF, OLA, and OA into toluene held in an ice bath. Initially, The end product consists of short, bullet-like NRs that develop into narrower NWs with a diameter of 2.6 nm after 24 hours at room temperature and thick nanowires of 6.1 nm diameter after one week. Ultimately, in 2018, Zhang et al. [23] purposefully included water in the fabrication of $CsPbBr_3$ PNCs by LARP, showing its impact on the crystal growth rate and morphology. According to the authors, hydroxonium (H_3O^+) and hydroxyl ion (OH^-) may function as ligands with more activity than oleylammonium and oleate species. As a result, PNCs began to expand in various orientations.

The LARP approach has certain drawbacks, even though it allows for the direct synthesis of numerous distinct perovskite complexes at room temperature. The polar solvents (DMF) that are typically employed in the LARP method have an inherent propensity to break down and even dissolve the CsPbX, particularly $CsPbI_3$ PNCs, because of their high sensitivity to polar solvents [21]. Interactions between the precursor and the polar solvent were found to be crucial in the development of faulty perovskite NCs. Zhang et al. [23] examined the consequences of utilizing various polar solvents on the crystallization of $MAPbI_3$ NCs to clarify this so-called "solvent effect". They demonstrated that PbI_2 produces stable intermediate species when dissolved in coordination solvents such as DMSO, DMF, and THF, but there is no formation of intermediates when noncoordinating solvents such as acetonitrile andbutyrolactone are used [68]. These crucial binding forces have various effects on the crystal structure of the thus-formed PNCs. There is a formation of faulty $MAPbI_3$ nanocrystals that have iodine vacancies in the bulk and residual solvent molecules on the periphery due to solid bonding between PbI_2 and coordinating solvents. When non-coordinating solvents are used, PbI_2 crystallizes into $MAPbI_3$ PNCs, which are defect-free. Additionally, the typical polar solvents (DMF and DMSO) employed in this method are high boiling point liquids and are poisonous, thus making them unsuitable for large-scale synthesis [69].

Halide Ion or Anion Exchange Method

An additional way to alter the optical characteristics and composition of PNCs while retaining their size and shape is through a post-preparative halide ion exchange method. Lignos and colleagues [32] and Shamsi et al. [21] investigated this method together to tune the emission of $CsPbX_3$ NC systems to have high PLQYs of 20–80%. Hybrid $MAPbBr_3$ PNCs, which were fabricated, also showed evidence of such anion exchange [20] and then combined with either the Cl or I form of methyl ammonium halide to create $MAPbBr_{3-x}Cl_x$ or $MAPbBr_{3-x}I_x$ PNCs [72]. The UV-visible absorption and photoluminescence emission confirmed how this halide exchange reaction controlled the composition, revealing the tenability of the band gap across the visible range. Yang and colleagues have proved that the anion exchange also happens in the solid state [73]. After growing in the solution phase, $MAPbBr_3$ nanorod arrays were annealed at 140–150 °C in MAI vapor to produce $MAPbI_3$ with a comparable shape. While the $MAPbI_3$ emits at

782 nm, the $MAPbBr_3$ nanorod assembling manifests green luminescence at 533 nm and full-width half maximum (FWHM) of 26 nm. Huang et al. [74] showed that injecting OLA along with OA and adjusting the reaction temperature enhanced control of the size distribution of $MAPbBr_3$ NCs.

Cation Exchange Method

For manipulating the composition of premade PNCs and accessing innovative nanostructures, the process of cation exchange, in which cations of preformed PNCs are replaced with new cations, has become a highly potent tool [43]. These modifications enable the creation of nano heterostructures or alloyed NCs using conventionally produced NCs as templates while maintaining the size distribution and morphology of rear crystals [74]. Cation exchange (CE) reactions can entirely or partially replace the A and B-cations in PNCs [43]. As A-cations make only a tiny contribution to the state's density close to the Fermi level, their influence on the band gaps of LHPs is negligible. The symmetry of the PNCs may, however, be significantly influenced by the type of A-cation. For instance, organic cations (FA^+ OR MA^+) have more tendency to bind with $[PbBr_6]_4$ octahedra through H-bonding. Therefore, symmetrical changes in LHPNCs can be induced when organic cations substitute inorganic cations by cation exchange, eventually influencing the vibrational modes [75]. In addition, modifying the A cations in LHPNCs can influence the tolerance factor, which in turn affects the stability of NCs, the position and duration of the PL peaks, and the dimensions of PNCs. For instance, by employing FA-oleate as a precursor, Cs^+ ions can be exchanged with FA^+ cations to produce more stable PNCs with a near IR emission [43]. When an FA-acetate salt is added to a solution of $MAPbX_3$ nanocrystals, a solid-liquid-solid cation exchange reaction can also produce $FAPbX_3$ NCs [76]. Octadecyl ammonium (OA^+) is substituted with Cs^+ or FA^+ in OA_2PbBr_4 micro platelets to make 2D perovskites, which results in a restructuring of the lattice. $[PbBr_6]^{4-}$ octahedra undergo corner sharing during this procedure, forming sheets with green emission with a 3D phase and possessing excellent optoelectronic and crystallinity features [77]. Although the exact cause of this 2D to 3D change, in which A-cations take the place of organic cations in the layered structures, is unknown, constructing a 3D network is thought to be responsible. The EN of B and X atoms increases with decreasing unit cell volume, and this is known to cause the band gap to increase [78].

To adjust the optical characteristics of LHPNCs, the post-synthetic substitute method is utilized in which B-cation is exchanged. It is understandable why the cation exchange of the B ions in LHPs is challenging to obtain, given that six halide ions surround Pb^{2+}ions (creating $[PbX6]^{4-}$ octahedra) and 8 A-cations. However, when using MBr_2 solutions dissolved in OLA/toluene, a partial cation exchange between PNCs ($CsPbBr_3$) and various metal cations is noted [79]. The absorption and emission spectra of the formed alloyed $CsPb1\text{-}xMxBr_3$ PNCs manifest blue-shift; the parent PNCs show remarkable PLQYs and narrow PL line widths (80 meV). The lattice contraction caused by MBr6 octahedra, which shows electrical decoupling from the PbBr6 framework, was explained to be the cause of the observed blue shift. The shorter bond length between Pb and Br and greater interaction forces between the Pb and Br orbitals result from the contraction of the $PbBr_6$ octahedra [80]. A more vital contact between the two atoms causes the maximum conduction band to move to higher energy, which widens the band gap. This is because the conduction band minimum (CBM) comprises antibonding (6p) orbitals of Pb and

(4p) orbitals of Br. Like the AE method, it was hypothesized that halide vacancies in the parent $CsPbBr_3$ PNCs made the CE process possible. In a nutshell, OLA molecules eliminate Br^- ions from the surface and also from $PbBr_2$ one at a time, leaving vacancies, which in turn facilitate the exchange of M^{2+} and Pb^{2+} ions. Then, MBr_2 species diffuse inside the lattice and occupy the open spaces [80]. The schematic sketch of this method is given in Fig. 4.

CE can also be used as an alternative method to create alloyed $CsPbxMn1\text{-}xCl_3$ PNCs with the same morphology and crystalline structure as the parent $CsPbCl_3$ NCs. Interestingly, by treating "as prepared" $CsMnCl_3$ PNCs with a solution of $PbCl_2$ solution after being dissolved in OLA, OA, and ODE, the exchange between Pb2+ and Mn2+ is entirely reversible. However, the production of pure $CsPbCl_3$ from $CsMnCl_3$ by CE is not feasible, due to the equilibrium established when Pb^{+2} ions are diffused inside, and Mn^{+2} ions are diffused outside [77]. This equilibrium presents a significant challenge in our research. Photo oxidation is a severe problem for these alloyed NCs. Interestingly, Liu et al. [39] synthesized $CsPbxMn1\text{-}xCl_3$ NCs enclosed in a matrix of KCl and proposed a dual ion exchange procedure for protecting NCs from oxidation caused by light and thermal degradation. The cation and anion exchange process produced $CsPbBr_3$ NCs when subjected to salts like $MnCl_2$ and KCl. Since the rigid structure of the halide octahedron surrounding Pb is likely to be opened during the exchange of halide ions, a partial interchange of Pb and Mn is expected to occur. Duration of reaction, intermediate core-shell structures with triple emission bands, and doping processes that rely on the composition of the dopant molecule are just a few of the unusual phenomena caused by this peculiar exchange property. Since it is very challenging for big $MnCl_2$ species to diffuse from the periphery to the center of the halide NCs, the exchange needs an extraordinarily longer time of 40 hours [44].

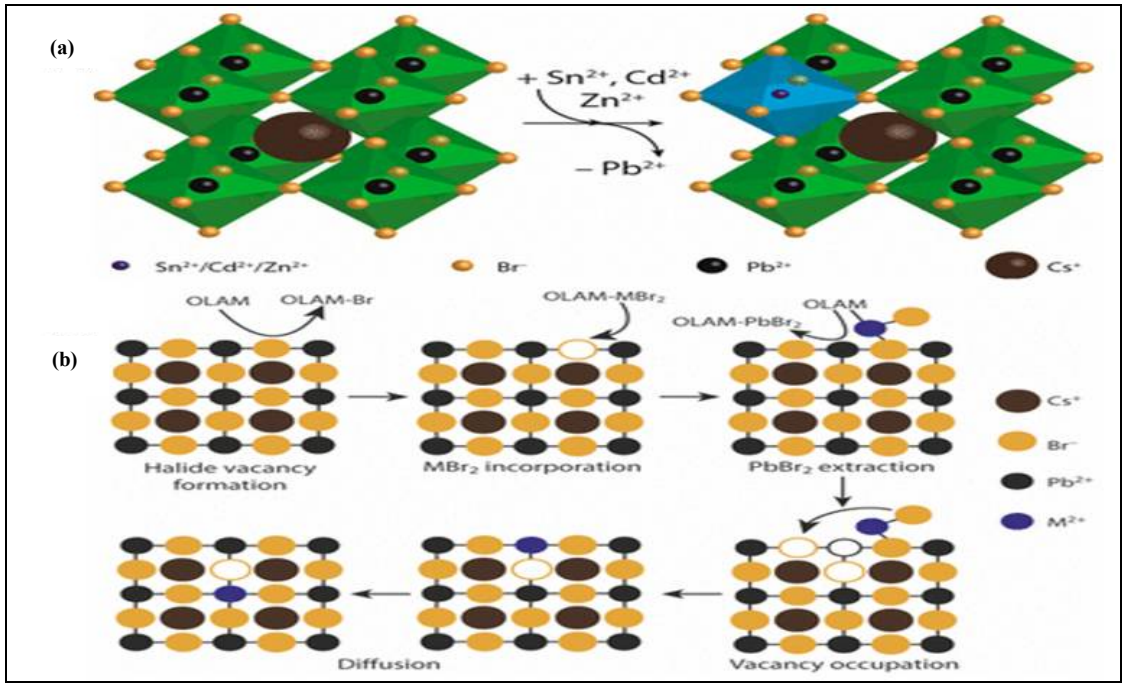

Figure 4. **(a) Partial $Pb^{2+} \rightarrow M^{2+}$ CE in $CsPbBr_3$ PNCs and the (b) Reaction Mechanism. Reproduced from ref [32]. Copyright 2019 American Chemical Society**

These challenges highlight the complexity and depth of our research. Similarly, by combining presynthesized $CsPbBr_3$ and $CsPb_{1-x}$ $MnxCl_3$ halide PNCs in hexane, a successful co-substitution reaction occurred. This reaction led to the formation of homogeneous Cs (PbxMn1-x)(ClyBr1-y)$_3$ nanocrystals, a significant achievement in our research [81]. In $CsPb(ClyBr_{1-y})_3$ enriched with Br, anion exchange is significantly greater than cation exchange and is responsible for the proliferation of Mn^{2+} substitution [82]. Similar reasoning was used to create Cs (Pb1-x-zZnz) (ClyBr1-y)$_3$:xMn^{2+} NCs that produce white light after being carefully mixed with $ZnBr_2$ (dissolved in OLA/hexane) [82].

Solid-state synthesis technique

Polycrystalline materials are created using a technique called solid-state synthesis. Since this approach synthesizes most ceramics, it is sometimes called the ceramic method. Researchers most frequently employ this method. This process needs raw materials that are carbonates or oxides in nature. The raw components don't interact chemically in this process at room temperature. A swift reaction occurs when the mixture of materials is subjected to a very high temp (700-1500 °C) [83].

Ball-Milling

Mechanical ball milling is employed to produce bulk PNCs. By adopting this method, perovskites are made by repeatedly grinding, mixing, ball milling, and burning the raw materials. The raw materials necessary to create the oxides and carbonate forms are ground, manually combined, milled, and heated. Let's use the perovskite phosphor $Ca_{0.97}$-xTiO_3:3Yb^{3+}, xBi^{3+} as an example to go over the entire process of this production method. TiO_2, Yb_2O_3, and Bi_2O_3 were employed as the starting ingredients for the production of $CaCO_3$. These components were first weighed in stoichiometric amounts, then manually ground and combined for one to two hours in a mortar using a pestle [83]. These were then ball milled to achieve homogeneity after mixing and grinding the initial ingredients for 4–12 hours at 25–100 rpm in clockwise and counterclockwise orientations. The homogeneous product following the ball milling was dried at room temperature, then separated into distinct sections for calcination at various temp between 600 -1500 °C for 4 to 30 hours to achieve the purest phase. This was followed by structural and optical characterization of the phosphors [83]. The perovskites made with this technique have sub-micrometer-sized particles [84]. This approach was also used to produce certain additional R0.5Ba0.5CoO_3 perovskites that were doped with rare earth [85].

High energy ball-milling method is highly comparable to the mechanical ball-milling method. But this approach uses very small-sized balls at extremely high rpms between a few hundred and several thousand. In this method, the oxide NPs are synthesized at low temperatures. The nanoparticles are commonly produced using this process. Because there is a very high likelihood that reactions will occur during high-intensity ball milling and produce harmful gases. Let's now discuss the procedure using the 0.7 $BiFeO_3$-0.3 $PbTiO_3$ solid solution as an example [86]. To make BF-PT, fixed ratios of Bi_2O_3, Fe_2O_3, PbO, and TiO_2 were combined. After this, the raw materials were ball-milled for 12–30 hours at 300–1000 rpm using zirconia balls and alcohol as the mixing medium in a 1:10 ratio with the sample. Since it could cause damage to the milling jars and O-rings, acetone or acid is not used here to combine the raw components [85]. To maximize the purity, the material was annealed at different temperatures (400–900 °C) after being dried at

90 °C. The samples' XRD patterns were recorded to verify the purity of the product formed. After annealing, the sample was combined with a 2% aqueous solution of PVA as a binder and converted into a pellet for further characterization. The PVA binder was burned out by firing the Perovskite pellet at 500 °C for 10–12 hours [82]. The pellet was sintered considerably higher than annealing temperatures to create the highly dense perovskite material. After sintering, the XRD pattern was captured further to verify the samples' purity. This technique is occasionally used to reduce the particle size from the micrometer to the nanometer range.

Gas-state Synthesis Technique

The nanoparticles are also created using a gas-state synthesis process. It employs furnaces, flames, plasmas, and lasers to manufacture oxide NPs. Although the fundamentals of thermodynamics and the reaction rates are incredibly alike, their reactors differ. The nanoparticles are distributed narrowly using these approaches. The dispersion must be decreased for a narrow distribution of NPs because it causes the particle size to grow [81]. A bottom-up methodology for creating multifunctional nanoparticles is gas-state synthesis. Collecting nanoparticles from smaller components is the foundation of the bottom-up nanofabrication method. These methods are entirely distinct from other synthesis methods and are used to generate thin films for various electrical instruments and solar cells made of perovskites. There are a variety of gas synthesis techniques like CVD, molecular beam epitaxy (MBE), laser ablation, DC sputtering, magnetron sputtering, thermal evaporation, and electron beam evaporation [81]. The gas-state synthesis process requires a particular setup and high-quality samples to provide the desired features. There are three different categories of gas-state synthesis methods:

1- Fabrication in a suitable environment condition at the crystallization temperature
2- Fabrication at a temperature between 500 and 800 °C; after this, annealing occurs at a higher temperature.
3- Fabrication with a post-annealing procedure at a very high temp after extremely low substrate temperature fabrication.

Table 1. **Advantages and disadvantages of the various methodologies used to synthesize PNCs.**

Methods	Advantages	Disadvantages	References
Hot-Injection Method	• High crystallinity • Controlled size and shape	• Requires high temperature • Sensitive to air and moisture	[25]
Halide Ion Exchange Method	• Allows for post-synthesis modification. • Tunable optical properties. • Retains morphology of original NCs	• Potential for incomplete exchange • Can introduce defects	[75]
LARPApproach	• Simple and fast • Good for large-scale production	• Lower crystallinity • Organic solvent residue	[24]
Cation Exchange Method	• Versatile for modifying composition • Maintains NCs size and shape	• Can be slow • Potential for incomplete exchange	[75]
Solid-State Synthesis Technique	• Solvent-free process • Potential for large-scale production • High purity	• High temperatures required • Limited control over NCs size and morphology	[26]
Gas-State Synthesis Technique	• High purity • Excellent control over composition • Suitable for thin films	• Complex equipment • High cost • Requires vacuum environment	[24]

The gas-state processes used to create perovskite materials have a variety of uses, including photocatalysts, solar cells, optical coatings, capacitors, semiconductors, bio-implantable devices, chemical reactors, and catalysts. It goes without saying that in the years to come, there will be a rise in industrial interest in creating technologies based on nanomaterials through gas-state synthesis [24]. Table 1 provides a comprehensive display of the benefits and drawbacks of the diverse methodologies employed in synthesizing PNCs.

Properties of Perovskite Nanocrystals
Crystal Structure

Lead halide PNCs (Fig. 5a) exist in the cubic $APbX_3$-type structure or its octahedral variants. These lattices are interconnected in three-dimensional (3D) space by their $[PbX_6]^{4-}$ octahedra, with the A-site cation present in large voids in between. These usual cubic or orthorhombic symmetries are vivid in the common cubic structures of the LHPNCs (Fig. 5b). As indicated by the idea of the Goldschmidt tolerance factor, which asserts close-packing of ions, only MA, FA, and Cs ions have the potential to stabilize the 3D PbX_6 lattice because of their geometric suitability inside a twelve-coordinate A-site. Larger or smaller cations approbate the genesis of low dimensional polymorphs (0D, 1D, or 2D), having the edge- or face-shared octahedra, resulting in bigger indirect energy bandgaps. Unlike the oxide perovskite NCs, LHPs show much lower melting points (400–500 °C in the case of $CsPbX_3$) owing to lower ionic charges, more considerable interatomic distances, and their higher inclination to thermal decomposition (below 300 °C for MA- and FA LHPs) [27].

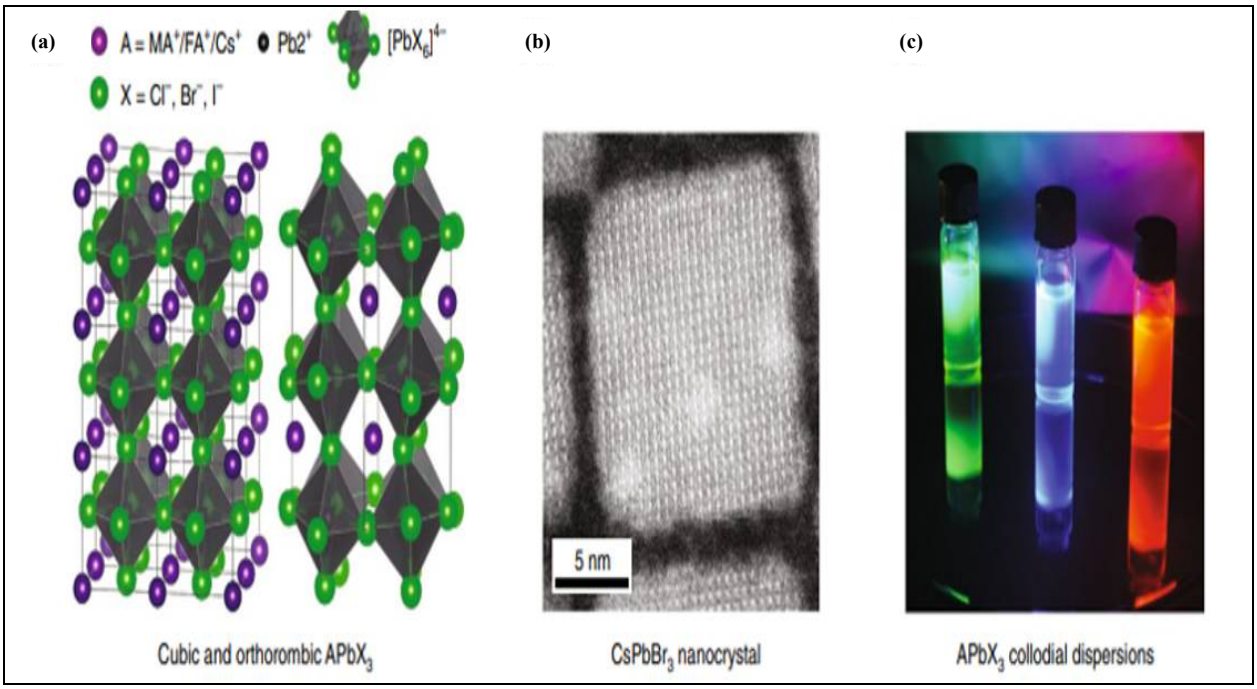

Figure. 5. **Colloidal LHPNCs. (a): Graphical representation of two typical structures of $APbX_3$ perovskite NCs , cubic (MAPbX3, FAPbX3) on the left and orthorhombic (CsPbX3) on the right. (b):(HAADF-STEM) photographs of a single, cubic CsPbBr3 NC, with 15-nm edge length. (c): the image of colloidal LHPNCs showing high luminescence (from left to right, CsPbBr3 with an emission peak at 520 nm, $CsPb(Cl/Br)_3$ show emission at 450 nm, and FAPb(Br/I)3 showing emission at 640 nm). Reprinted with permission by ref [30], copyright 2018 Nature Materials**

Optical and Electronic Characteristics of LHPs

The extraordinary performance of LHPNCs, particularly in photovoltaic and LEDs, depends heavily on their excellent optical characteristics. Certain Perovskite materials have incredibly high absorption coefficients; the maximum penetration depth of $MAPbI_3$ was calculated to be 0.66 μm for 550 nm and 2.0 μm for 700 nm, respectively. $MAPbI_3$'s absorption coefficient was 1.5 × 104 cm^{-1} at 550 nm and 0.5 × 104 cm^{-1} at 700 nm. Compositional engineering allows the MHPs' absorption peaks to gradually change to cover the visible spectrum. According to theoretical calculations, the p subshell of lead primarily contributes to the CBE. In contrast, the p orbital of the halides, which are hybridized with varying amounts of lead states, predominate the valence band maximum (VBM) of the $MAPbX_3$ PNCs [71]. Therefore, altering the metal ions or halides can alter the MHP's VBM, CBM, and bandgap [76].

The energy band structure is also minutely affected if organic cations are changed. This is because the bond length and bond angle of (B-X) can fluctuate depending on the organic cation present at the A-site. For instance, by changing the (FA) cation with (MA) in the $MAPbI_3$ perovskite, the bandgap can be reduced from 1.64 eV to 1.43 eV. Because of their resilience towards defects and low non-radiative recombination, perovskite nanocrystals exhibit sound, light emission, and superior light-absorbing properties. MHPs are particularly appealing for usage in LEDs and lasers due to the ease with which basic solution processes can be used to create MHP emitters with almost unity PLQY. By manipulating the composition, it is also feasible to change their PL peaks, and one of the most significant benefits of perovskites over other semiconductor substances is their versatility in optical properties depending on the composition [49].

Soon after the presentation of the first report on $MAPbBr_3$ NCs, which had absorption onset and a PL emission around 529 nm, it was elaborated that changing the halide composition could change the optical properties of such NCs throughout the entire visible spectrum, earlier noted for bulk Perovskite thin films. Protesescu et al. [24] demonstrated that the emission wavelength for $CsPbX_3$ (with X = Cl, Br, or I) nanocrystals could be shifted from 410 nm (X = Cl) to 512 nm (X = Br) to 685 nm (X = I), virtually going through all values in between by using mixed halide components, represented in Fig. 6.

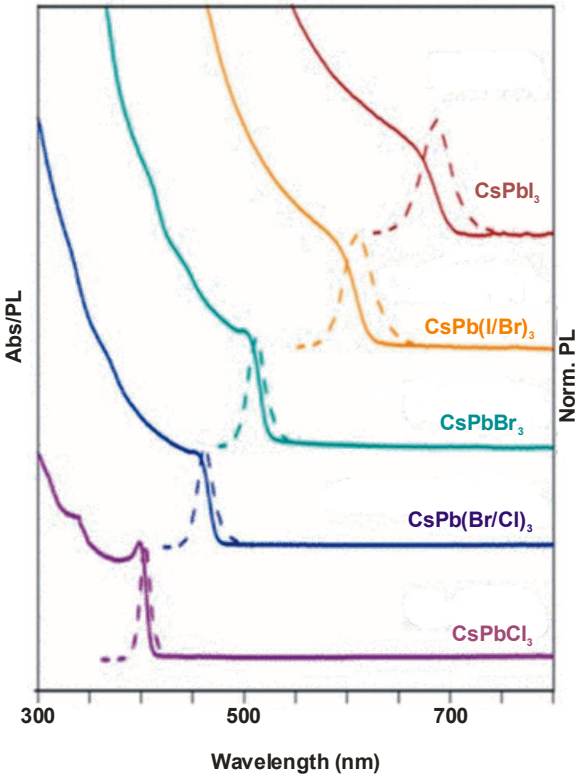

Figure 6. **Representation of tunability in the band gap of $CsPbX_3$ NCs as a function of halide content, as manifested by UV–vis and PL spectra. Reproduced from ref [49], copyright 2019 American Chemical Society**

For the use of MHP in optoelectronic devices, carrier mobility, diffusion length, and carrier lifetime are essential. Carrier mobility

describes how easily charge carriers can flow through a substance. The lifetime specifies the duration required by the airlines for recombination, and the diffusion length measures the distance they move by diffusion. Since they directly impact how well the corresponding devices work, those factors are frequently considered in MHP materials. Surprisingly, MHPs have extraordinarily long diffusion lengths that range from (1 to > 170 μm) owing to their chemical makeup, shape, and structure of the device. At the same time, a massive crystal of MHP showed carrier mobility (10 $cm^2V^{-1}s^{-1}$). With the development of film deposition, morphological control techniques, and device structure optimization over the past ten years, the electrical characteristics of MHPs have significantly improved, resulting in increased device performance [49].

Over the past decade, Perovskite light-emitting diodes (PeLEDs) employing cesium lead halide have made significant advancements, achieving external quantum efficiencies (EQEs) exceeding 20% from a mere 0.1%. Initially limited to low temperatures (~77 K), these thin film-based PeLEDs became viable for everyday use in 2014 and they are used in multicolor operation at ambient temperature with EQEs below 1%. Researchers subsequently focused on enhancing efficiency through methods such as morphology control, composition adjustments, and device innovation [52]. Gao et al. [76] notably achieved electroluminescence (EL) in green, blue, and orange using $CsPbX_3$ nanocrystals, with current efficiencies reported at 0.43 cd/A, 0.14 cd/A, and 0.08 cd/A, respectively. The EL from organometallic lead halide perovskite-conjugated polymer diodes was explored, highlighting efficient EL comparable to LEDs in 3D inorganic-organic perovskite materials, provided that the electron and hole currents are balanced within the perovskite materials. Recent advancements in metal halide PeLEDs have shown remarkable progress. Zhang et al. [61] conducted investigations on high-efficiency metal halide PeLEDs with significantly improved light extraction on nanophotonic substrates, achieving an external quantum efficiency of 17.5%, nearly twice the previous record for planar devices using this material system. Their findings indicate that employing nanophotonic structures can be a viable strategy for producing high-performance perovskite optoelectronic devices. The band structure engineering explored through various dimensions, compositions, and external stimuli. Hu et al. [26] demonstrated $CsPbBr_3$ nanoplate devices with an EQE of around 0.2%, proposing applications in on-chip integrated photonics. The study was done on the pivotal role of inorganic mixed halide PNCs in technological frontiers and explore the impact of iodine incorporation into $CsPbBr_3$ nanocrystals, highlighting significant shifts in X-ray diffraction (XRD) peaks that indicate structural changes affecting their optical properties. The introduction of iodine alters the bandgap energy, influencing light absorption and emission behaviors, and enhancing their suitability for diverse optoelectronic applications. $CsPbX_3$ PNCs' tunable optical properties through halide composition adjustments highlight how variations in $CsPbBr_3$ and $CsPbBr_2I$ structures affect their structural and optical characteristics. The average crystallite size of approximately 21.8 nm plays a crucial role, with smaller sizes potentially leading to quantum confinement effects that further improve optical performance. Moreover, the diligent efforts of researchers have yielded positive outcomes in the form of efficiency figures surpassing 20%, as recently reported. Despite these initial promising advancements, challenges such as long-term stability under operational conditions remain critical, particularly due to the sensitivity of perovskite

structures to moisture, leading to phase transitions and degradation issues like phase segregation in mixed halide perovskites, which affect device reliability and performance [47].

Defect Tolerance

LHPs are quite unusual because they have an excellent defect tolerance, though highly dense structural defects exist. Fortunately, these defects are entirely contained within either the VB or CB and not in the band gap, so a clean band gap is preserved upon the emergence of common defects like vacancies or surface-related sites owing to their highly luminescent nature and without employing any surface passivation, contrarily traditional QDs made from metal chalcogenides require passivation to produce a high PLQY. Theoretically, the defect tolerance had been explained for various perovskite compounds. For $CsPbBr_3$ NCs surfaces, for example, point defects on bulk material and grain boundaries were all demonstrated to occur in the valence band and conduction band or to produce shallow trap states. We can say that the defect tolerance in perovskite NCs originates from three essential attributes: crystal structure, which results in the generation of vacancies but no other point defects; electronic structure, which leads to benign vacancies; and their dynamic lattice effects (creation of polarons), thus preventing carrier traps [83].

This defect tolerance in LHPs coincides with several factors described above. Although there is a large variety of point defects, only vacancies (A- and X-site) (Fig. 7a) are exclusively observed as these have extremely low formation energies. Interstitial and antisite defects are almost absent because ions in the perovskite structure are easily misplaced. The shallow character of the states due to vacancies is because of the peculiar nature of bonding in LHPs, namely the antibonding character of the valence band maxima (with mixed halide 3/4/5p and Pb 6s character; Fig. 7b) and spin–orbit effects in the conduction band (which has a predominant Pb 6p character). NC surfaces can be regarded as the planes of vacancies and thus manifest benign behavior as vacancies. Consequently, high-photoluminescence (PL) quantum yields (QYs) without surface passivation in LHPNCs are observed.

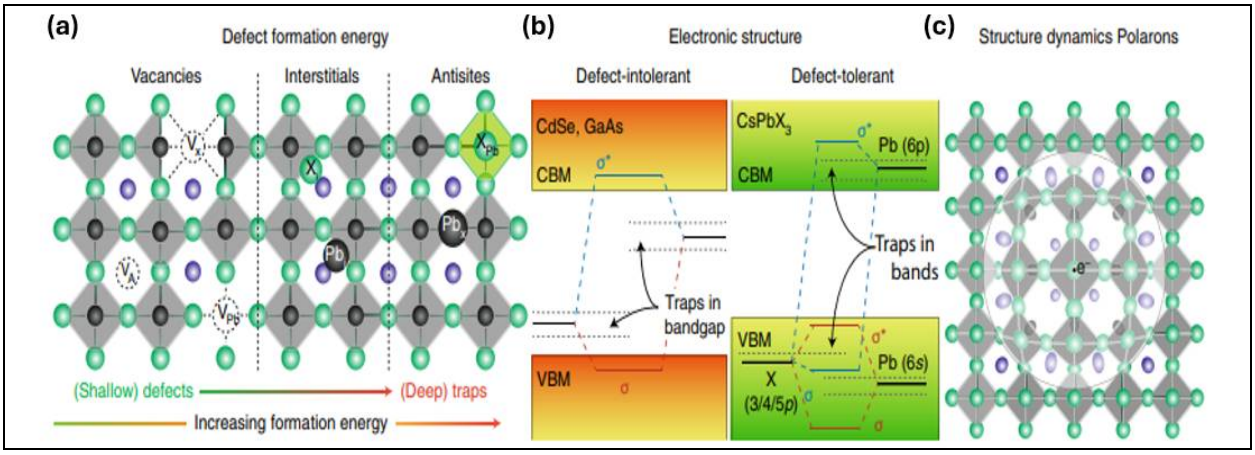

Figure 7. **Defect Tolerance in LHPs: (a) typical point defect (vacancies, interstitial, and antisite atoms) to increase formation energy and depth in the bandgap. (b), graphical comparison of the electronic band structure of defect-intolerant semiconductors and LHPNCs (c), schematic illustration of local structural deformation of the Pb–Br framework in association with a charge carrier (electron or hole), which creates a polaron. Reprinted with permission from ref [30], copyright 2018 Nature Materials.**

The bandgap is created between bonding (σ) and antibonding (σ*) orbitals in typical semiconductors, such as cadmium chalcogenides. Point defects or dangling bonds originate as weak bonding or non-bonding states within the bandgap. In LHPs, the bandgap is formed between two antibonding orbitals. So, defect states are created from only shallow traps or entrapped in the conduction or valance band and will not strongly influence radiative recombination and other optical characteristics [83]. Due to the soft and dynamic nature of the perovskite structure, this material is considered a crystalline liquid. These properties protect its carriers from trapping and scattering. Also, due to its partial ionic character, the intense structural features of PbX lattices at room temperature led to the formation of polarons (Fig. 7c). These polarons help to shield the Coulombic potential and lessen-trapping and carrier scattering, both mutually and with charged defects and optical phonons [83].

Similarly, defect tolerance is anticipated to be highly relevant in 2D Perovskites. Even when several ligands are removed from the surface, NCs can still be light solid emitters, and the impact of the resulting surface defects on trapping charge carriers is in Perovskite quantum dots, trap states or defects are in the conduction or valence band, thus having an insignificant effect on photoluminescence. Therefore, lead halide QDs can demonstrate 90% PLQY, unlike traditional quantum dots. Shelling with broad band gap semiconductors is not necessary to boost their PLQY. Though lead halide perovskite NCs have magnificent defect tolerance, it does not mean that they are defect-free, as $CsPbX_3$ QDs show 80-95% PLQY in the green-red region and 10 –20% in the blue region [71]. Due to the adequate low formation energy, vacancies are frequently seen, especially in the A- and X-sites. As a result of unique ionic bonding in perovskite QDs, these vacancies result in shallow defect states (for example, 0.5 eV in PNCs as opposed to $CaTiO_3$, which shows 2-3 eV. However, compared to other non-passivated chalcogenide QDs, the defect tolerance and PLQY of Perovskite quantum dots are far up, and research in post-synthesis by ligands and doping results in the PLQY of Perovskite quantum dots to be close to 100%. Overall, a complete insight into the exceptional defect tolerance in LHPs has not yet been gained [23].

Structure Liability, Stability Issues, and Enhancement Strategies for PNCs

Commercial photovoltaic (PV) systems predominantly use silicon technology, which is favored for its high and stable efficiency, reaching up to 26.7%, and a robust lifespan, often guaranteed for up to 20 years. These efficiencies are consistently reproducible through established and standardized manufacturing processes. On the other hand, Perovskite-based solar cells have shown significant potential, achieving peak PCEs above 80% of their theoretical maximum of 30%, corresponding to a bandgap of 1.6 eV, in less than a decade of development. Despite these advances, their practical application remains limited to laboratory-scale devices, typically with absorber areas of less than 1 cm^2.

The broad adoption of Perovskite solar cells is hampered by both extrinsic and intrinsic stability issues. Extrinsic issues, such as sensitivity to humidity and oxygen, can be addressed through established encapsulation methods. However, intrinsic challenges, including thermal instability and ion migration, stem from the chemical nature of the absorber material itself. These intrinsic factors result in complex interdependencies between the material properties and the device fabrication processes, posing significant

challenges to the wider technological implementation of Perovskite absorbers [87]. The stability of perovskite nanomaterials and their constituent devices significantly impacts their performance and potential for future commercialization. The Perovskite crystal structure comprises a metal halide octahedral framework that is prone to distortion and deterioration in different environmental conditions. Factors like defects and impurities such as vacancies, interstitials, and dopants further exacerbate the instability of the crystal structure, leading to structural disarray and alterations in the material's electronic characteristics. In addition to their intrinsic instability, Plasmonic Nanocrystals are linked to the ligand capping through electrostatic interactions. The ligands play a pivotal role in the stabilization of PNCs and in the prevention of their aggregation. Nevertheless, the association between PNCs and ligands is inherently precarious, leading to potential detachment of ligands from the nanocrystals. The surface ligands of $CsPbBr_3$ nanocrystals exhibited a highly dynamic nature, suggesting that the ligands in the Perovskite nanocrystal solution might not be strongly bound to the nanocrystal surface. There exists a rapid interchange between the unbound and bound states of the ligands, rendering them susceptible tobe lost during the process of separation and purification [83].

LHPNCs are terminated by Oleyl ammonium bromide or Oleyl ammonium carboxylate [25]. Ammonium groups substitute A-site cations present on the surface, while carboxylates act as anions. These ligands tend to desorb fast (Fig. 8a). The difficulties encountered while isolating and purifying colloids using typical procedures for QDs are repeated precipitation that occurs in the presence of non-solvent preceded by redispersion in the presence of a pure solvent— these are the most dramatic effects of loose ligand binding. The ligands having different anchoring groups, like zwitterionic molecules comprising quaternary ammonium and carboxylate groups, may exhibit more static surface coordination (Fig. 8b). It is also possible to imagine oligomeric ligands with charged groups and elongated hydrocarbon chains per molecule. Due to its ionic solid character and low lattice energy, LHPs are moderately soluble in almost all organic solvents of polar nature; in reality, this causes LHPNCs to dissolve eventually. Until a method for utterly encapsulating LHPNCs in an inert shell is developed (within the silica, titania, alumina, and salts with deficient solubility products such as $BaSO_4$ or similar, as shown in Fig. 8c, it will be cumbersome to solve this issue.

However, a traditional method for covering LHP PNCs with SiO_2 would call for customizing a sol-gel procedure like the Stöber method. This has not yet been shown, most likely because alcohols or other protic polar solvents are required. Due to the fragility of LHPNCs, complex shapes like the existence of core-shell nanocrystals and other nanocrystals heterostructures have not yet been proven. The critical problem with $MAPbX_3$ lead halide PNCs is its intrinsic chemical instability; although it is much lesser than $FAPbX_3$, it is still significant. So $MAPbX_3$ compounds are characterized by low formation energy, and thus, they decompose even at room temperature. According to reports, the high surface area of the NCs and other factors such as heat, light, moisture, and oxygen speed up this decomposition, producing PbX_2 and several volatile compounds (CH_3NH_2, HI, I_2, and other species). Another significant obstacle for almost all potential uses of LHPNCs is poor thermal stability. $MAPbI_3$ at around 150–200 °C and $FAPbI_3$ disintegrate before melting in hybrid organic–inorganic LHPs. The MP of (AI) PNCs ($CsPbBr_3$ and $CsPbI_3$) are greater (450–500 °C) to some degree than

those of organic LHPs (290–300 °C). As a result, all LHPNCs have a high sintering susceptibility. Any device fabrication that depends on preserving quantum confinement in a closely packed assemblage of LHPNCs or for high-temperature devices like lasers or remote phosphors faces a significant hurdle. In red-emitting $CsPbI_3$PNCs, another type of structural liability has been identified. The Cs+ ions are too tiny to fit inside a 3D Perovskite lead iodide cage, resulting in the change from one polymorph to another, which has lower dimensions and, as a result, a wider bandgap [34].

On the other hand, it has also frequently been stated that altering the purification process and excluding air during maneuver and storage do lengthen the life of the metastable (3D $CsPbI_3$) stage [41]. Many efforts have been made to stabilize $CsPbI_3$ by restricted replacement of Cs^+ with (FA^+) and partial replacement of I^- with Br^-, both using NCs and thin films [41]. Similar stability effects were noted when smaller cations like Mn^{2+} and Bi^{3+} were used instead of Pb^{2+}, as evident by the retention of the vivid red PL. Beyond solution-phase chemistry, a further untapped potential may merit consideration, particularly in light ofstabilizing LHPs under thermal and environmental conditions. It may be toughto cover lead halide PNCs with crystalline shells orstructurally stable interfaces, according to dynamic disorder in structure on fs-ps timescales. The melt-growth of lead halide PNCs, which are glass-embedded, as seen in recent findings using conventional phosphate or borosilicate glasses, is a possible alternate route to stable LHP emitters Fig. 8d [54]. The resulting NCs, whose size is adjusted by melt-quenching thermal conditions, are covered by a chemically stable glass matrix impenetrable to air and water. Such glass-embedded NCs can be incorporated into LHP emitters' display backlighting and remote phosphors. Grinding after cooling the melt can quickly obtain them in powdered form.

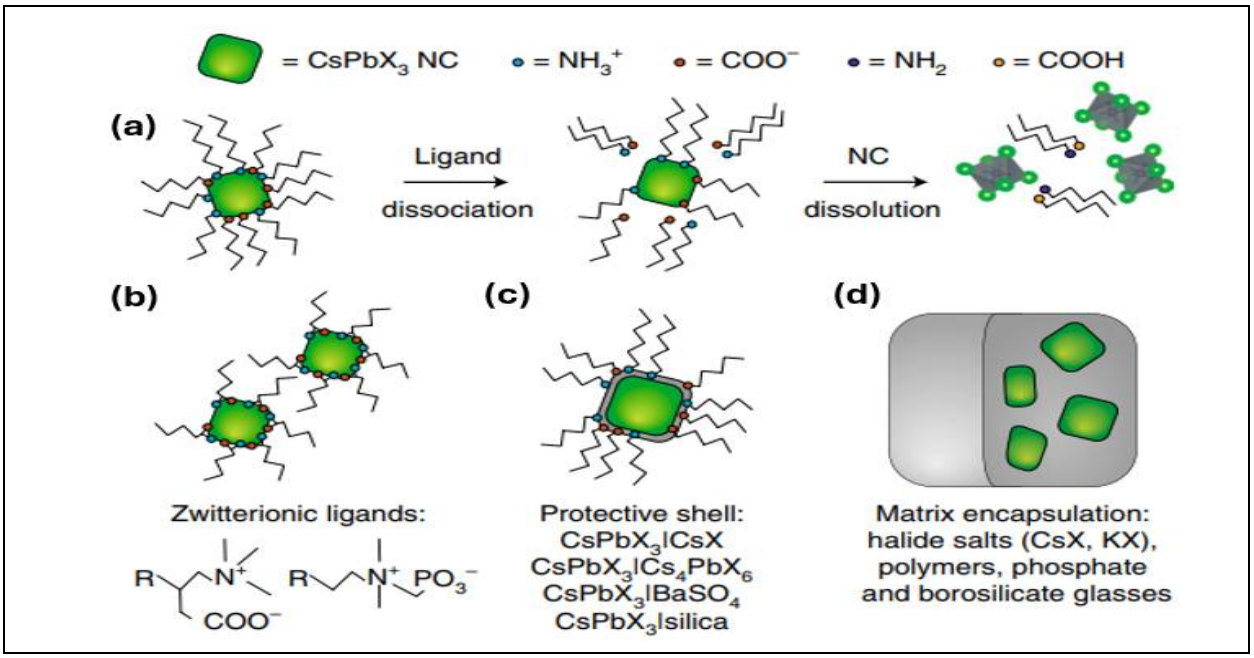

Figure 8. **Structural liability of LHPNCs and stabilization methods. (a) loss of colloidal stability due to the desorption of weakly bound ligands. b–d, strategies to achieve stable surface coverage by ligands (b) employing zwitterionic molecules, (c) overcoating with dielectric shells or compositionally matched salts, and (d) matrix encapsulation into polymers or crystalline and amorphous inorganic matrixes. Reprinted with permission from ref [27], copyright 2018 Nature Materials**

Environmental factors such as moisture, oxygen, and light significantly influence the stability of PNCs. Exposure to humidity causes perovskite grains to change color from black to yellow and undergo a phase transition from α-phase to δ-phase due to water infiltration through surface defects. This interaction with MA^+ forms weak hydrogen bonds, leading to structural degradation from a three-dimensional to a zero-dimensional system. Additionally, oxygen presence in the atmosphere affects stability, with prolonged light exposure inducing color shifts in $CsPbBr_3$ nanocrystals from green to yellow, indicating degradation. Haque et al. proposed that photostimulation generates charge carriers, and oxygen diffusion forms superoxide species that degrade perovskite. Protective strategies like encapsulation mitigates H_2O and oxygen ingress, yet continuous light exposure remains challenging for long-term stability in perovskite-based optoelectronic devices. Phase transitions in MAPbI3−xBrx films were observed under continuous illumination, demonstrating the impact of environmental conditions on Perovskite stability [56].

Encapsulation has become a leading method for improving the stability and performance of PNCs, increasingly adopted by researchers. Organic polymers like polystyrene-block-poly(acrylic acid) (PS-bPAA) and inorganic materials such as silica dioxide are utilized to encapsulate PNCs, enhancing their suitability for commercial applications. Using PS-bPAA to stabilize PNCs effectively, a method was developed, creating polymer capsules through methanol-assisted phase separation in toluene. This approach is particularly effective for Cs-oleate-coated nanocrystals, reducing toxicity and improving stability against water [67]. Additionally, Chen et al. [13] introduced alcohol-resistant polyacrylic acid-capped $CsPbBr_3$ PNCs (PAA-PNCs) with internal polystyrene (PS) shells, achieving high uniformity, durability against environmental stressors, and maintaining fluorescence efficiency. However, the encapsulation layer may affect light extraction efficiency in optoelectronic applications, depending on the polymer type and technique used. These advancements underscore the expanding role of encapsulation in enhancing PNC functionality and applicability in various fields, including biotechnology and photonics. Silica encapsulation has emerged as a promising strategy to enhance the stability of hybrid organic–inorganic PNCs. Yu et al. [70] utilized tetramethoxysilane to form silica composites via hydrolysis in ammonia, resulting in $CsPbBr_3/SiO_2$ particles with uniform dispersion and minimal aggregation. The (3-aminopropyl) triethoxy-silane for on-site silica encapsulation of $CsPbBr_3$ nanocrystals employed on hydrophobic PVDF membranes [73] demonstrated significant fluorescence retention under high-humidity conditions. The 3-aminopropyl triethoxysilane was utilized to encapsulate α-FAPbI3 nanocrystals, achieving stable white LEDs with high color gamut [76]. Despite enhancing stability, silica encapsulation may reduce light extraction due to potential light scattering and could limit flexibility in applications requiring mechanical resilience. These approaches highlight silica as a versatile encapsulation material for improving the durability of PNCs in diverse optoelectronic and photonic applications. Recent advancements in encapsulation techniques for PNCs have introduced a variety of innovative materials. Gao et al. [76] demonstrated using bone gelatin as a capping agent for $CsSnCl_3$ nanocrystals, achieving high stability with preserved PL intensity and improved quantum yield compared to uncapped counterparts [76]. The graphitic carbon nitride (CNM) was employed for in situ encapsulation of $CsPbBr_3$ nanocrystals, enhancing stability in the air, water, and polar

solvents over two months while maintaining fluorescence characteristics. Wang et al. [2] utilized ethyl α-cyanoacrylate monomer octavinylsilsesquioxane (OVS) to create superhydrophobic–polymer composites, achieving enhanced chemical stability and quantum efficiency. Additionally, Zhang et al. employed ZSM-5 hierarchically structured zeolite (HSZ) for thermal diffusion encapsulation, offering outstanding water resistance and prolonged luminescent behavior in $CsPbBr_3$ nanocrystals. These developments highlight diverse strategies to improve the durability and functionality of PNCs across various technological applications [61].

Organic ligands play a crucial role in stabilizing PNCs like $CsPbBr_3$ by passivating their surfaces, enhancing stability, solubility, and PL intensity. However, interactions between ligands and bromide ions can sometimes lead to destabilization. The ligand engineering approach involves tailoring organic molecules to anchor onto PNC surfaces effectively. Liu et al. [39] demonstrated this with their LARP technique, which synthesizes $CsPbBr_3$ nanocrystals under ambient conditions, achieving high PLQY and stability through precise ligand interactions [71]—Similarly, analogous methods with different ligands were employed, achieving stable PNCs suitable for various applications. Recent studies have highlighted significant advancements in enhancing the stability and performance of polymeric nanocomposites through ligand engineering [81]. Lee et al. [9] utilized organic semiconductor and modified polyacrylic acid ligands to improve the stability and photoluminescence efficiency of $CsPbBr_3$ nanocrystals. Liu et al. [39] employed AHDA ligands to enhance the environmental durability of $CsPbI_3$s, while Minh et al. [57] utilized 1-octadecanethiol ligands to preserve crystal phase integrity. Inorganic ligands such as tungstosilicic acid (TSA), as demonstrated by Zhang et al. [23] have also proven effective in modifying CsPbBr3 nanocrystals, enhancing stability and retaining luminescence after extended storage [84]. a silver–trictylphosphine complex WAS introduced to produce robust $Cs_2Ag_{1-x}NaxInCl_6$ double PNCs resistant to solvents, showcasing advancements in stabilizing unconventional PNCs. These studies underscore the critical role of tailored ligands in optimizing PNC properties, though challenges in synthesis complexity and variability necessitate precise control and selection of ligands for consistent results [25].
Metal cation doping is a frequently employed method to boost the stability of PNCs. For example, there is an achievement in the synthesis of highly luminescent, green-emitting zinc-doped cesium lead titanate nanocrystals, which remained stable in high-humidity environments using the LARP method [65]. The incorporation of zinc adjusted the bandgap, passivated Pb^{2+} defects, and improved the material's stability. Nazim's research on Cr^{3+} doping in hybrid organic–inorganic metal halide PNCs revealed that Cr^{3+} cations could partially replace Pb^{2+} ions, thereby enhancing optical properties and maintaining thermal stability and cubic geometry [76]. A low-temperature method was developed for synthesizing $CsPb_2Br_5/CsPbBr_3$ PNCs doped with transition metals such as Ni^{2+}, Cu^{2+}, and Zn^{2+}. This doping approach effectively eliminated bromine vacancies and suppressed nonradiative recombination, leading to higher PLQY and enhanced stability. Specifically, Ni^{2+}-doped nanocrystal films showed notable water stability, while Cu^{2+}-doped nanocrystals exhibited exceptional thermal stability,

resulting in high luminescence across the visible spectrum [27]. Recent advancements in perovskite nanocrystal synthesis have focused on enhancing stability and performance through innovative techniques. High-entropy alloying was explored to stabilize lead-reduced metal halide perovskite nanocrystals, achieving improved colloidal stability, narrow-band emission, and high PLQY [81]. Liu et al. [39] successfully synthesized Al^{3+}-doped $Cs_2AgBiCl_6$ nanocrystals, enhancing fluorescence by shifting from indirect to direct bandgap characteristics while maintaining exceptional stability over extended periods [2]. Gao et al. [76] utilized $DMAPbX_3$ and n-octylamine for surface passivation to produce high-quality $CsPbBr_3$− nanocrystals with 92% PL quantum efficiency and excellent stability. Additionally, it was demonstrated the use of DMSO doping in α-$CsPbI_3$ synthesis for efficient perovskite solar cells with a notable 10.6% power conversion efficiency using a PEDOT:PSS hole-transporting layer. These studies highlight diverse strategies—from alloying and doping to precise precursor engineering—that significantly advance the optical and structural properties of perovskite nanocrystals for various applications [33].

Applications of LHPs

LHPNCs are widely recognized for their various applications in optoelectronic devices owing to their distinct crystal structure and exceptional optoelectronic properties. These nanocrystals find utility in an array of devices such as solar cells, photodetectors, LEDs, lasers, displays, X-ray detectors, and even in photocatalytic applications. Recent studies have demonstrated that through the manipulation of stoichiometric ratios of precursors and integration of anion exchange reactions, the emission characteristics of these nanocrystals can be precisely adjusted throughout the visible spectrum, spanning from violet to green and red [17].

LCDs

Due to their narrow emission bandwidths, LHPNCs provide high PLQYs and highly saturated colors, essential for LCDs. Semiconductor NCs' symmetric and narrow emission bands offer outstanding color purity compared to organic dye molecules. In contrast, LHPNCs provide an exceptional gamut with 140% of the NTSC specification. Also, LHPNCs can be utilized as color-down converters in LCD backlighting. Polymer films with red and green LHPNCs embedded in polymer beads can be employed. Barrier films with low oxygen and water transfer rates can be used in such devices to ensure high PLQY. CdSe or InP-based NCs have already been implemented by several significant display manufacturers, including Sony, Samsung, and LG. Si and GaAs are two other well-known semiconductors that can emit in the green and red regions. However, it is difficult to manage their PL characteristics since it is difficult to make high-quality colloidal NCs. Regarding brightness, color range, stability, and power consumption, green-emissive InP NCs and CdSe or LHPNCs still operate very differently [17]. Given the intrinsic restrictions of control of shape and compositional homogeneity, CdSe-based NCs and LHPNCs continue to be excellent candidates to defeat InP. LHPNCs already provide red and green emission FWHM values of 20 and 35 nm, respectively [63].

LEDs

The broad color spectrum of the photoluminescence of LHPNCs satisfies the present color criterion for display applications (Fig. 9a). The small PL FWHM of ≤100 meV

in $CsPbBr_3$, and $FAPbBr_3$ NCs is by only 18–20 nm in the green region near 520–530 nm, making them valid competitors of conventional green phosphors. Other applications are remote phosphors for lighting, color control, and color-enhancement films in portable devices. In display applications, employing LHPNCs in optically transparent polymers or an inorganic matrix is a vivid approach for achieving thermal and environmental stability. Magnificent outcomes on the long-term stability of such emitters were gained by implementing LHPNCs in water-impermeable polymers and into salt matrices, such as potassium halides or Cs_4PbBr_6. The electronic surface passivation is not needed for LHPNCs, and this aspect is helpful for charge carrier injection in light-emitting diodes (Fig. 9b). So, $CsPbBr_3$ LEDs are extensively studied, with external quantum efficiencies (EQEs) of 6.3% and 8.7%. In the former case, there was a peak luminance of over 15,000 cd m^{-2}, whereas the latter observed a moderate value of 1,660 cd m^{-2}. Both studies emphasize the significance of purifying LHPNCs from excess ligands. Red $CsPbI_3$ NC LEDs observed an EQE of 7.3% and a peak luminance of 435 cd m^{-2} at 688 nm [31].

The prominent characteristics sought in the next generation of high-quality LEDs encompass several key aspects: (i) superior color quality featuring a wide color gamut, narrow emission full width at half maximum (FWHM), and enhanced brightness, (ii) elevated EQE and current efficiency (CE), and (iii) an optimal low-temperature solution-based fabrication process, which could significantly reduce both the economic and energetic expenditures involved in their production. Presently, conventional inorganic LEDs employing rare-earth phosphors and epitaxial III–V semiconductors can mimic natural light and lead to substantial energy conservation, albeit at the expense of high manufacturing outlays, necessitating processing in an inert environment at high temperatures and employing costly substrates. These challenges can be mitigated by leveraging perovskite nanocrystals as emitters in LEDs (PeLEDs) due to the facile nature of their solution-based processing, cost-effective precursor materials, inherently high PLQY, and notably, a high tolerance towards defects. Notably, perovskite nanocrystals present exceptional color purity, surpassing the emission FWHM narrowness observed in typical organic light-emitting diodes (OLEDs). The compact nature of red, green, and blue (RGB) LEDs renders them invaluable as light sources for various display applications. Several key attributes of select PeLEDs are predicated on using PNCs. PeLEDs have witnessed remarkable enhancements in EQEs, progressing from levels below 0.1% to exceeding 20%. While initial investigations predominantly concentrated on "bulk" or thin-film perovskite emitters, it became evident that PNCs offer distinct advantages for PeLEDs. The reduced dimensions and size of these nanocrystals augment the exciton binding energy and diminish the diffusion length, thereby averting current leakage in LEDs, a phenomenon absent in the context of sluggish electron-hole bimolecular radiative recombination observed in bulk perovskite materials. Furthermore, surface modification enables the optimization of semiconductor properties of perovskite nanocrystals [64].

Solar Cells

LHPs have garnered considerable attention in the realm of solar cell applications owing to their exceptional optoelectronic characteristics, which encompass high carrier mobility, a band gap that is tunable, and absorption coefficients of a high magnitude. The aforementioned materials have demonstrated a noteworthy power conversion

efficiency, evidenced by the fact that certain lead halide-based perovskite solar cells have achieved efficiencies exceeding 20% within a relatively brief timeframe. The predominant focus of research on perovskite solar cells has been on polycrystalline films rather than on devices that are manufactured from nanocrystals [83]. As of the year 2018, Perovskite thin films had recorded PCEs, which are defined as the ratio between incident solar power and the useful output electrical power in a solar cell surpassing the 22% mark. A viable strategy for the creation of efficient solar cells involves utilizing perovskite nanocrystal solutions as "inks" and transforming them into continuous films through a combination of solution-based and thermal treatment methods. Despite exhibiting promising performance metrics, concerns regarding stability have been flagged, potentially posing a constraint on their commercial feasibility. Strategies aimed at bolstering stability encompass the incorporation of buffer layers and the manipulation of additives, with the overarching goal of suppressing degradation reactions and enhancing the longevity of the devices [39].

Lasers

LHPNCs have exhibited considerable potential in the realm of laser applications. Previous studies have illustrated the fabrication of low-threshold single-mode vertical-cavity surface-emitting lasers (VCSELs) utilizing $CsPbBr_3$ NCs, resulting in the achievement of single-mode lasing at 527 nm with a pulse duration of approximately 10 ps. The influence of lead halide nanocrystals, including $CsPbBr_3$ and $CsPbI_3$, on laser efficacy is noteworthy owing to their distinctive characteristics. These nanocrystals demonstrate size-dependent anti-Stokes photoluminescence, with superior efficacy observed in smaller nanocrystals like 6 nm methylammonium lead bromide NCs, ascribed to interactions between electrons and phonons and radiative recombination through excitonic states [47]. Moreover, the employment of $CsPbBr_3$ nanocrystals as a saturable absorber in erbium-doped fiber lasers (EDFL) has facilitated passively Q-switched laser operation in the C-band region, resulting in the generation of pulses as brief as 5.96 μs with commendable stability. Furthermore, the customization of optoelectronic properties and stability of lead halide perovskite nanocrystals via chemical engineering has culminated in the production of pure blue emissive PNCs with augmented photoluminescence quantum yield and stability, demonstrating promise for applications in information security [58]. The amalgamation of $CsPbBr_3$ nanocrystals with a minor quantity of Cd can effectively neutralize halide vacancies, thereby enhancing stability and bolstering the strength of electron-phonon coupling, which subsequently leads to reduced ASE thresholds and enhanced photostability. Additionally, the optimization of surface ligand species for $CsPbBr_3$ nanocrystals yields narrow photoluminescence line shapes, bulk-like Stokes shifts, and diminished inhomogeneous broadening, facilitating their integration into nanophotonic structures for advanced quantum optical analyses [53].

Bioimaging

Lead halide nanocrystals, specifically $CsPbX_3$ (X= Cl, Br, I), have exhibited significant potential in bioimaging applications due to their exceptional photophysical attributes. The encapsulation of these nanocrystals within water-soluble polymer capsules has been devised to amplify their stability and biocompatibility, thereby facilitating a heightened photoluminescence quantum yield that can endure over prolonged durations. Moreover, the amalgamation of LHPNCs with lanthanide-doped nanoparticles

has yielded steadfast, near-infrared excitable, and emission-tuneable materials, rendering them apt for biological applications. Encased lead halide perovskite nanocrystals have manifested luminous emission when subjected to one- and two-photon excitation, alongside fortified stability in aqueous and biological mediums, rendering them well-suited for both in vitro and in vivo bioimaging applications. Furthermore, $CsPbBr_3$ nanocrystals enclosed within functionalized polyethylene glycol have demonstrated exceptional photostability, narrow emission spectra, and high spatial resolution, positioning them as optimal candidates for single molecule localization microscopy in cellular imaging [78].

The encapsulation of perovskite NCs utilizing diverse functionalized polymers is an alternative technique for shielding the core perovskite materials against harsh external conditions. Varied bio-compatible polymer-coated perovskite NCs have often been favored to ensure minimal cytotoxicity, heightened stability, and facile uptake within cells. Polyvinylpyrrolidone (PVP) polymer incorporates a profoundly hydrophilic pyrrolidone moiety and hydrophobic alkyl groups, which deter the aggregation of NCs owing to their repulsive forces. PVP engenders an exceedingly thin shell encasing the NCs' surface through adsorption, which can readily detach under external duress. An additional appropriate coating/binding encompassing PVP-coated NCs is imperative to sustain the particle size and enhance crystal stability, a crucial aspect for practical bioimaging applications [55].

Recently, PVP polymers have been harnessed as a surfactant to stabilize the $CsPbX_3$ NCs and have also functioned as an interfacial layer to render them compatible with the coating of PMMA and polystyrene (PS) polymers. Nevertheless, the dimensions of these nanocomposites are notably large (~mm range) due to the unregulated polymer coating over the PVP layer, diminishing the efficacy of cellular uptake. Poly[n-isopropyl acrylamide] (pNIPAM) is a widely researched thermosensitive biocompatible polymer characterized by a lower critical solution temperature, extensively utilized as a polymer hydrogel in the realm of biomedical applications, including cancer cell imaging, drug delivery systems, and biosensors [80].

Biosensors

Engaging in the detection, quantification, and subsequent removal of environmental contaminants is imperative to adequately safeguard the ecosystem, as these actions play a crucial and indispensable role in ecological protection. In this context, the synthesis and fabrication of innovative nanomaterials and nanocomposites emerge as pivotal components in advancing diverse analytical methodologies to combat pollution. Specifically, metal halide perovskites, encompassing both inorganic and organic-inorganic varieties and their corresponding composites, have emerged as highly effective tools for quantitatively analyzing a wide array of analytes. The unique sensor responses exhibited by $CsPbX_3$ are primarily attributable to its exceptional electro-optical characteristics, which significantly contribute to the advancement of various semiconducting and sensing applications. Notably, $CsPbX_3$ demonstrates remarkable chemical stability even at elevated temperatures surpassing 350 °C while also showcasing a vibrant emission characterized by a high PLQY exceeding 90%. Moreover, the bandgap of $CsPbX_3$, spanning between 1.7 and 3 eV, can be precisely modulated within the visible spectrum by adjusting X-site ions and composition ratios, thereby enabling the realization of emissions ranging from red to blue [76].

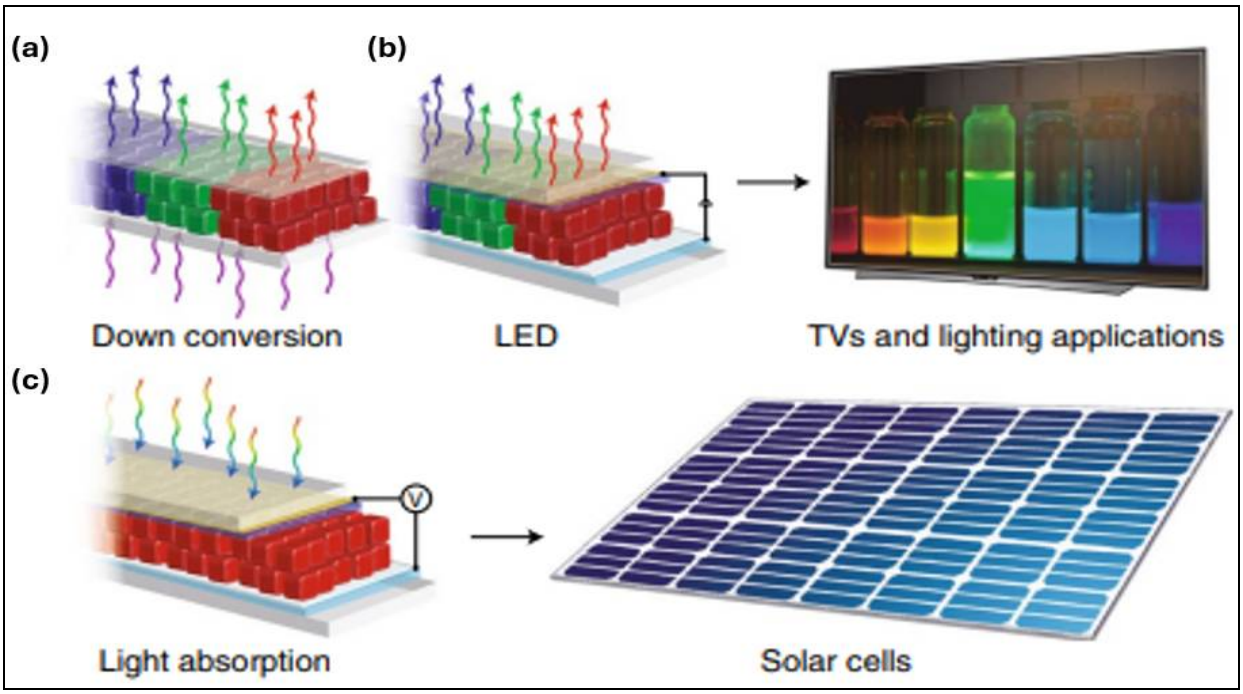

Figure. 9 **Optoelectronic applications of LHPNCs. LHPNCs are used in (a) PL down conversion, (b) LEDs, and (c) solar cells. Reprinted with permission from ref [30] Copyright 2018 Nature Materials**

Photocatalysis

Over the past few decades, the exponential growth in energy consumption has led to many environmental and energy-related challenges, including issues such as water contamination, air pollution, and the greenhouse effect. These crises have necessitated the exploration of innovative solutions on a global scale. Among the various strategies proposed, photocatalysis has emerged as one of the most promising and sustainable methods for addressing these pressing concerns. Recently, there has been a surge of interest in applying PNCs $CsPbX_3$ for photocatalytic purposes. These nanocrystals have garnered significant attention due to their exceptionally high PLQY, superior charge carrier mobility, extended carrier lifetime, tunable band gap based on size, remarkable absorption capacity, and diverse chemical processabilities. The groundbreaking research conducted by Kovalenko and collaborators laid the foundation for the synthesis of colloidal $CsPbX_3$ PNCs, sparking a wave of endeavors aimed at exploring the potential applications of $CsPbX_3$ Perovskite as photocatalysts [73].

Researchers have directed their efforts towards utilizing $CsPbX_3$ Perovskite in various photocatalytic processes, such as hydrogen evolution, organic dyestuff degradation, and CO_2 reduction in aqueous and ethyl alcohol environments. For example, $CsPbBr_3$ NCs have been engineered specifically for hydrogen production, while the development of Ag-$CsPbBr_3$/CN composite materials has shown promise in degrading organic pollutants [65].

Conclusion

Metal halide Perovskites are now the focus of research because of their potential applications in photovoltaics and unique optoelectronic properties. The evolution of novel colloidal methods for the amalgamation of LHPs and their fascinating properties have attracted the attention of many researchers.

Our review has focused on various colloidal synthesis methods for synthesizing PNCs with the chemistry and the efficiency of these colloidal approaches concerning manipulating the resulting nanocrystals' shape, size, and optical characteristics. Efficient pure-color or white-light LHPs will likely become an excellent commercial opportunity shortly. Combining the essential attributes of colloidal LHPNCs and bulk 2D perovskites to gain 'multidimensional 3D/2D' LHPNCs is a fascinating field of research, where electronic structure is tailored on both the atomic scale and nanoscale [26]. However, the operational lifetime of these devices is still minimal, and a complete understanding of degradation processes has not yet been achieved. Perovskite is implemented in LEDs andphosphors, yet conventional quantum dots have already dominated this commercial field. Other main issues are Pb toxicity and the inherent instability of the perovskite structure. The future of perovskites is very bright, but there are still many challenges ahead for the applicability of this magic material in real-life applications outside a research laboratory [86].

Declaration statement

The authors affirm that they possess no identifiable conflicting financial concerns or personal associations that could have conceivably affected the research presented - in this manuscript.

References

1. R. J. Tilley, *MRS Bull.*, 42 (2017) 325. doi:10.1557/mrs.2017.81
2. Y. Wang, J. Liu, Y. Liu, S. Li , X. Xu and Z. Lou, *J. Mater. Chem. C*,12 (2024) 10267. doi:10.1039/D4TC01556H
3. D. Weber, Z. *Naturforsch. B*, 34 (1979) 939. doi:10.1515/znb-1979-0712
4. D. Weber, *Z. Naturforsch. B*, 33 (1978) 862. doi:10.1515/znb-1978-0809
5. D. B. Mitzi, L. W. Lombardo, A. Kapitulnik, S. S. Laderman and R. D. Jacowitz, *Phys. Rev*. B, 41 (1990) 10. doi.org/10.1103/PhysRevB.41.6564
6. T. Miyasaka, A. Kulkarni, G. Kim, M, S. Öz and A.K. Jena, *Adv. Energy Mater.*, 10 (2020) 1902500. doi:10.1002/aenm.201902500
7. J. H. Rhee, C. C. Chung and E. W. G. Diau, *NPG Asia Mater.*, 5 (2013) e68. doi: 10.1038/am.2013.53
8. A. Soosaimanickam, *Handbook of Emerging Materials for Semiconductor Industry*, Springer, (2024) 693. doi.org/10.1007/978-981-99-6649-3
9. M. M. Lee, J. Teuscher, T. Miyasaka, T. N. Murakami and H. J. Snaith, *Sci.*, 338 (2012) 643. doi: 10.1126/science.1228604
10. S. M. Yoo, S. J. Yoon, J. A. Anta, H. J. Lee, P. P. Boix and I. Mora-Sero, *Joule*, 3 (2019) 2535. doi: 10.1016/j.joule.2019.07.014
11. A. Kojima, K. Teshima, Y. Shirai and T. Miyasaka, *J. Am. Chem. Soc.*, 131 (2009) 6050. doi.org/10.1021/ja809598r
12. R. A. Deshpande, *J. Sci. Res.,* 65 (2021**)** 72. doi: 10.37398/JSR.2021.650214
13. J. K. Chen, Q. Zhao, N. Shirahata, J. Yin, O. M. Bakr, O. F. Mohammed and H.T. Sun, *ACS Mater. Lett.*, *3* (2021) 845. doi: 10.1021/acsmaterialslett.1c00197
14. Q. Zhang, M. He, Q. Wan, W. Zheng, M. Liu, C. Zhang and L. Li, *Chem. Sci.,* 13 (2022) 3719. doi:10.1039/D1SC06554H
15. N. G. Park, *Mater. Today,*18 *(*2015) 65. doi:10.1016/j.mattod.2014.07.007
16. E. Mosconi, P. Umari and F. De Angelis, *Phys. Chem. Chem. Phys.*, 18 (2016) 27158.

doi : 10.1039/C6CP03969C
17. H. Huang, M. I. Bodnarchuk, S. V. Kershaw, M. V. Kovalenko and A. L. Rogach, *ACS Energy Lett.*, 2 (2017) 2071. doi : 10.1021/acsenergylett.7b00547
18. S. A. Khan, N. Z. Khan, M. Sohail, M. Runowski, X. Xu and S. Agathopoulos, *Mater. Today Phys.*, 34 (2023) 101079. doi:10.1016/j.mtphys.2023.101079
19. I I. Levchuk, A. Osvet, X. Tang, M. Brandl, J. D. Perea, F. Hoegl and C. J. Brabec, *Nano Lett.*, 17 (2017) 2765. doi: 10.1021/acs.nanolett.6b04781
20. K. H. Wang, L. Wu, L. Li, H. B. Yao, H. S. Qian and S. H. Yu, *Angew. Chem.*, 128 (2016) 8468. doi: 10.1002/ange.201602787
21. J. Shamsi, P. Rastogi, V. Caligiuri, A. L. Abdelhady, D. Spirito, L. Manna and R. Krahne, *ACS Nano*, 11 (2017) 10206. doi.10.1021/acsnano.7b04761
22. C. Witt, A. Schmid, N. Leupold, M. Schultz, J. Höcker, A. Baumann, R. Moos and F. Panzer, *ACS Appl. Electron. Mater.*, 2 (2020) 2619. doi.org/10.1021/acsaelm.0c00493
23. F F. Zhang, H. Zhong, C. Chen, X.-G. Wu, X. Hu, H. Huang, J. Han, B. Zou and Y. Dong, *ACS Nano*, 9 (2015) 4533. doi: 10.1021/acsnano.5b01154
24. L. Protesescu, S. Yakunin, M. I. Bodnarchuk, F. Krieg, R. Caputo, C. H. Hendon, R. X. Yang, A. Walsh and M. V. Kovalenko, *Nano Lett.*, 15 (2015) 3692. doi: 10.1021/nl5048779
25. K.Vighnesh, S. Wang, H. Liu and A. L. Rogach, *ACS Nano*. 16 (2022) 19618. doi:10.1021/acsnano.2c11689
26. S. Hu, J. Thiesbrummel, J. Pascual, M. Stolterfoht, A. Wakamiya and H. J. Snaith, *Chem. Rev.*, 124 (2024) 4079. doi:10.1021/acs.chemrev.3c00667
27. Q. A. Akkerman, G. Rainò, M. V. Kovalenko and L. Manna, *Nat. Mater.*, 17 (2018) 394. doi:10.1038/s41563-018-0018-4
28. Q. A. Akkerman, S. Park, E. Radicchi, F. Nunzi, E. Mosconi, F. De Angelis and L. Manna, *Nano Lett.*, 17 (2017) 1924. doi :10.1021/acs.nanolett.6b05262
29. I. Lignos, S. Stavrakis, G. Nedelcu, L. Protesescu, A. J. DeMello and M. V. Kovalenko, *Nano Lett.*, 16 (2016) 1869. doi: 10.1021/acs.nanolett.5b04981
30. R. M. Maceiczyk, K. Dümgen, I. Lignos, L. Protesescu, M. V. Kovalenko and A. J. deMello, *Chem. Mater.*, 29 (2017) 8433. doi:10.1021/acs.chemmater.7b02998
31. M. Koolyk, D. Amgar, S. Aharon and L. Etgar, *Nanoscale*, 8 (2016) 6403. doi: 10.1039/C5NR09127F
32. I. Lignos, L. Protesescu, D. B. R. Emiroglu, R. Maceiczyk, S. Schneider, M. V. Kovalenko and A. J. deMello, *Nano Lett.*, 18 (2018) 1246. doi: 10.1021/acs.nanolett.7b04659
33. Z. Dang, J. Shamsi, Q. A. Akkerman, M. Imran, G. Bertoni, R. Brescia and L. Manna, *ACS Omega*, 2 (2017) 5660. doi:10.1021/acsomega.7b01009
34. T. Udayabhaskararao, Y. Sun, N. Goswami, S. K. Pal, K. Balasubramanian and T. Pradeep, *Angew. Chem. Int. Ed.*, 51 (2012) 2155. doi.org/10.1002/anie.201107696
35. Y. Dong, T. Qiao, D. Kim, D. Parobek, D. Rossi and D. H. Son, *Nano Lett.*, 18 (2018) 3716. doi: 10.1021/acs.nanolett.8b00861
36. L. Yuan, R. Patterson, X. Wen, Z. Zhang, G. Conibeer and S. Huang, *J. Colloid Interface Sci.*, 504 (2017) 586. doi:10.1016/j.jcis.2017.06.017
37. J. Y. Woo, Y. Kim, J. Bae, T. G. Kim, J. W. Kim, D. C. Lee and S. Jeong, *Chem. Mater.*, 29 (2017) 7088. doi:10.1021/acs.chemmater.7b02669
38. Y. Zhao, A. M. Nardes and K. Zhu, *J. Phys. Chem. Lett.*, 5 (2014) 490. doi: 10.1021/jz500003v

39. P. Liu, W. Chen, W. Wang, B. Xu, D. Wu, J. Hao, W. Cao, F. Fang, Y. Li and Y. Zeng, *Chem. Mater.*, 29 (2017) 5168. doi:10.1021/acsami.7b10612
40. E. Yassitepe, Z. Yang, O. Voznyy, Y. Kim, G. Walters, J. A. Castañeda, P. Kanjanaboos, M. Yuan, X. Gong and F. Fan, *Adv. Funct. Mater.*, 26 (2016) 8757. doi: 10.1002/adfm.201604580
41. L. Protesescu, S. Yakunin, S. Kumar, J. Bär, F. Bertolotti, N. Masciocchi, A. Guagliardi, M. Grotevent, I. Shorubalko and M. I. Bodnarchuk, *ACS Nano*, 11 (2017) 3119. doi: 10.1021/jacs.6b08900
42. L. Protesescu, S. Yakunin, M. I. Bodnarchuk, F. Bertolotti, N. Masciocchi, A. Guagliardi and M. V. Kovalenko, *J. Am. Chem. Soc.*, 138 (2016) 14202. doi:10.1021/acs.nanolett.7b04838
43. S. E. Creutz, E. N. Crites, M. C. De Siena and D. R. Gamelin, *Nano Lett.*, 18 (2018) 1118. doi:10.1021/acs.nanolett.7b04059
44. M. Imran, V. Caligiuri, M. Wang, L. Goldoni, M. Prato, R. Krahne, L. De Trizio and L. Manna, *J. Am. Chem. Soc.*, 140 (2018) 2656. doi:10.1021/jacs.7b13477
45. Y. Tong, E. Bladt, M. F. Aygüler, A. Manzi, K. Z. Milowska, V. A. Hintermayr, P. Docampo, S. Bals, A. S. Urban and L. Polavarapu, *Angew. Chem. Int. Ed.*, 55 (2016) 13887. doi: 10.1002/anie.201605909
46. V. K. Ravi, N. Singhal and A. Nag, *J. Mater. Chem. A*, 6 (2018) 21666. doi: 10.1039/C8TA06126B
47. Y. S. Zhao, H. Fu, A. Peng, Y. Ma, D. Xiao and J. Yao, *Adv. Mater.*, 20 (2008) 2859. doi: 10.1002/adma.200800604
48. G. Xing, N. Mathews, S. Sun, S. S. Lim, Y. M. Lam, M. Grätzel, S. Mhaisalkar and T. C. Sum, *Science*, 342 (2013) 344. doi:10.1126/science.1243167
49. P. Arunkumar, K. H. Gil, S. Won, S. Unithrattil, Y. H. Kim, H. J. Kim and W. B. Im, *J. Phys. Chem. Lett.*, 8 (2017) 4161. doi: 10.1021/acs.jpclett.7b01440
50. Y. Zhao, X. Xu and X. You, *Sci. Rep.*, 6 (2016) 35931. doi: 10.1038/srep35931
51. S. A. Veldhuis, Y. K. E. Tay, A. Bruno, S. S. Dintakurti, S. Bhaumik, S. K. Muduli, M. Li, N. Mathews, T. C. Sum and S. G. Mhaisalkar, *Nano Lett.*, 17 (2017) 7424. doi: 10.1021/acs.nanolett.7b03272
52. A. Nikaki, C. Piperi, and A. G. Papavassiliou, *Expert Opin. Investig. Drugs*, 21 (2012) 1475. doi: 10.1002/adfm.201604018
53. M. B. Abid, L. Gzara, I. A. Moujdin, M. A. Salam and R. A. Wahab, *Polimery*, 69, 1 (2024) 44. doi.org/10.14314/polimery.2024.1.5
54. J. Shamsi, A. L. Abdelhady, S. Accornero, M. Arciniegas, L. Goldoni, A. R. S. Kandada, A. Petrozza and L. Manna, *ACS Energy Lett.*, 1 (2016) 1042. doi: 10.1021/acsenergylett.6b00521
55. S. W. Dai, B. W. Hsu, C. Y. Chen, C. A. Lee, H. Y. Liu, H. F. Wang, Y. C. Huang, T. L. Wu, A. Manikandan and R. M. Ho, *Adv. Mater.*, 30 (2018) 1705532. doi: 10.1002/adma.201705532
56. I. Levchuk, P. Herre, M. Brandl, A. Osvet, R. Hock, W. Peukert, P. Schweizer, E. Spiecker, M. Batentschuk and C. J. Brabec, *Chem. Commun.*, 53 (2017) 244. doi:10.1039/C6CC09266G
57. D. N. Minh, J. Kim, J. H. Hyon, J. Sim, H. H. Sowlih, C. Seo, J. Nam, S. Eom, S. Suk and S. Lee, *Chem. Mater.*, 29 (2017) 5713. doi: 10.1021/acs.chemmater.7b01705
58. J. Luo, X. Wang, S. Li, J. Liu, Y. Guo, G. Niu, L. Yao, Y. Fu, L. Gao, Q. Dong and C. Zhao, *Nature*, 563 (2018) 541.

doi: 10.1021/acs.nanolett.7b01544
59. X. Li, Y. Wu, S. Zhang, B. Cai, Y. Gu, J. Song and H. Zeng, *Adv. Funct. Mater.*, 26 (2016) 2584. doi: 10.1002/adfm.201670096
60. A. Kostopoulou, M. Sygletou, K. Brintakis, A. Lappas and E. Stratakis, *Nanoscale,* 9 (2017) 18202. doi: 10.1039/C7NR06404G
61. X. Zhang, X. Bai, H. Wu, X. Zhang, C. Sun, Y. Zhang, W. Zhang, W. Zheng, W. W. Yu and A. L. Rogach, *Angew. Chem. Int. Ed.*, 57 (2018) 3337. doi: 10.1002/anie.201710869
62. X. Li, D. Yu, F. Cao, Y. Gu, Y. Wei, Y. Wu, J. Song and H. Zeng, *Adv. Funct. Mater.*, 26 (2016) 5903. doi: 10.1002/adfm.201601571
63. F. Zhang, S. Huang, P. Wang, X. Chen, S. Zhao, Y. Dong and H. Zhong, *Chem. Mater.*, 29 (2017) 3793. doi:10.1021/acs.chemmater.7b01100
64. Q. A. Akkerman, V. D'Innocenzo, S. Accornero, A. Scarpellini, A. Petrozza, M. Prato and L. Manna, *J. Am. Chem. Soc.*, 137 (2015) 10276. doi: 10.1021/jacs.5b05602
65. D. M. Jang, K. Park, D. H. Kim, J. Park, F. Shojaei, H. S. Kang, J.-P. Ahn, J. W. Lee and J. K. Song, *Nano Lett.*, 15 (2015) 5191. doi: 10.1021/acs.nanolett.5b01430
66. A. B. Wong, M. Lai, S. W. Eaton, Y. Yu, E. Lin, L. Dou, A. Fu and P. Yang, *Nano Lett.*, 15 (2015) 5519. doi: 10.1021/acs.nanolett.5b02082
67. K. Hills-Kimball, Y. Nagaoka, C. Cao, E. Chaykovsky and O. Chen, *J. Mater. Chem. C*, 5 (2017) 5680. doi: 10.1039/C7TC00598A
68. V. A. Hintermayr, A. F. Richter, F. Ehrat, M. Döblinger, W. Vanderlinden, J. A. Sichert, Y. Tong, L. Polavarapu, J. Feldmann and A. S. Urban, *Adv. Mater.*, 28 (2016) 9478. doi: 10.1002/adma.201602897
69. D. Yu, B. Cai, F. Cao, X. Li, X. Liu, Y. Zhu, J. Ji, Y. Gu and H. Zeng, *Adv. Mater. Interfaces*, 4 (2017) 1700441. doi: 10.1002/admi.201700441
70. D. Yu, C. Yin, F. Cao, Y. Zhu, J. Ji, B. Cai, X. Liu, X. Wang and H. Zeng, *ACS Appl. Mater. Interfaces*, 9 (2017) 39602. doi: 10.1021/acsami.7b12048
71. D. Yu, F. Cao, Y. Gao, Y. Xiong and H. Zeng, *Adv. Funct. Mater.*, 28 (2018) 1800248. doi:10.1002/adfm.201800248
72. I. E. Castelli, J. M. García-Lastra, K. S. Thygesen and K. W. Jacobsen, *APL Mater.*, 2 (2014) 081514. doi: 10.1063/1.4893495
73. M. B. Abid, R. A. Wahab and L. Gzara, *J. Appl. Membr. Sci. Technol.*, 27, 2 (2023) 39. doi.org/10.11113/amst.v27n2.267
74. G. Huang, C. Wang, S. Xu, S. Zong, J. Lu, Z. Wang, C. Lu and Y. Cui, *Adv. Mater.*, 29 (2017) 1700095. doi: 10.1002/adma.201700095
75. W. Van der Stam, J. J. Geuchies, T. Altantzis, K. H. Van Den Bos, J. D. Meeldijk, S. Van Aert, S. Bals, D. Vanmaekelbergh and C. de Mello Donega, *J. Am. Chem. Soc.*, 139 (2017) 4087. doi: 10.1021/jacs.6b13079
76. D. Gao, B. Qiao, Z. Xu, D. Song, P. Song, Z. Liang, Z. Shen, J. Cao, J. Zhang and S. Zhao, *J. Phys. Chem. C*, 121 (2017) 20387. doi: 10.1021/acs.jpcc.7b06929
77. F. Li, Z. Xia, Y. Gong, L. Gu and Q. Liu, *J. Mater. Chem. C*, 5 (2017) 9281. doi: 10.1039/C7TC03575F
78. F. Li, Z. Xia, C. Pan, Y. Gong, L. Gu, Q. Liu and J. Z. Zhang, *ACS Appl. Mater. Interfaces*, 10 (2018) 11739. doi: 10.1021/acsami.7b18750
79. L. Zhang, Z. Xu, L. Cao and X. Yao, *Mater. Lett.*, 61 (2007) 1130. doi: 10.1016/j.matlet.2006.06.069

80. A. Upadhyay, R. Pandey and A. K. Singh, *J. Am. Ceram. Soc.*, 100 (2017) 1743. doi: 10.1111/jace.14735
81. P. Ring, *Prog. Part. Nucl. Phys*., 37 (1996) 193. doi.org/10.1016/0146-6410(96)00054-3
82. B. Kwak, K. Zhang, E. Boyd, A. Erbil and B. Wilkens, *J. Appl. Phys.*, 69 (1991) 767. doi: 10.1063/1.347362
83. Z. Yu, J. Ramdani, J. Curless, J. Finder, C. Overgaard, R. Droopad, K. Eisenbeiser, J. Hallmark, W. Ooms and J. Conner, *J. Vac. Sci. Technol. B*, 18 (2000) 1653. doi: 10.1116/1.591445
84. T. Imai, M. Okuyama and Y. Hamakawa, *Jpn. J. Appl. Phys.*, 30 (1991) 2163. doi: 10.1143/JJAP.30.2163
85. B. Yang, J. Y. Wang and Y. M. Jia, *Int. Conf. Thin Film Phys. Appl. SPIE,* 1519 (1991) 725. https://doi: 10.1117/12.47277
86. C. Lu and H. Shen, *Appl. Phys. A*, 67 (1998) 253. doi: 10.1007/s003390050767
87. Y. Li, X. Xu, C. Wang, C. Wang, F. Xie, J. Yang and Y. Gao, *AIP Adv.*, 5 (2015) 097111. doi: 10.1063/1.4930545